Neutralino decays in the minimal supersymmetric standard model

Sandro Ambrosanio* and Barbara Mele†
Dipartimento di Fisica, Università "La Sapienza" and Istituto Nazionale di Fisica Nucleare, Sezione di Roma, P.le Aldo Moro 2, I-00185 Rome, Italy
(Received 4 August 1995)

A complete phenomenological study of the next-to-lightest neutralino decays is performed in the MSSM. The widths and branching ratios for all the possible decay channels (including the radiative decay $\tilde{\chi}_2^0 \to \tilde{\chi}_1^0\gamma$ and the decay into a light Higgs boson $\tilde{\chi}_2^0 \to \tilde{\chi}_1^0 h^0$) are studied in detail as functions of all the SUSY parameters of the model. Particular attention is paid to situations that are interesting for searches at CERN LEP 2. Nontrivial decay patterns are found that critically depend on the region of the parameter space considered.

PACS number(s): 14.80.Ly, 12.60.Jv

I. INTRODUCTION

The introduction of supersymmetry (SUSY) can solve the hierarchy problems in the standard model (SM) only if SUSY is broken at the TeV scale. This implies that the SUSY partners of the known particles should be produced at e^+e^- and pp collider machines planned for the next years. The possibility of observing the new states depends not only on their production cross sections but also on their particular decays and consequent signatures that might or might not allow their detection in real experiments. Hence, a complete knowledge of the decay structure and relevant branching ratios (BR's) of the lightest SUSY states (the first that could be detected) is crucial for discussing the discovery potential of the different machines.

In the minimal supersymmetric standard model (MSSM) [1], among the lightest particles in the SUSY spectrum, there are 4 neutralinos [the SUSY partners of the neutral electroweak (EW) gauge and Higgs bosons] and two charginos (the partners of the charged gauge and Higgs bosons). In most scenarios, apart from the lightest SUSY particle (LSP), which is in general assumed to be the lightest neutralino ($\tilde{\chi}_1^0$) (stable and invisible), the particles that could be first observed at future experiments are the next-to-lightest neutralino ($\tilde{\chi}_2^0$) and the light chargino ($\tilde{\chi}_1^\pm$) [2]. In particular, the production of $\tilde{\chi}_1^0\tilde{\chi}_2^0$ pairs at e^+e^- colliders could allow the study of a wide region of the SUSY parameter space [3]. In this respect, it is crucial to know as well as possible the decay characteristics of the $\tilde{\chi}_2^0$, that determine the features of the observed signal.

Analytical results for the neutralino decay widths have been thoroughly studied in Refs. [4–7]. Nevertheless, at the present time, a complete phenomenological analysis that investigates the different kinematical and dynamical features of neutralino decays corresponding to different regions of the SUSY parameter space, is still missing to our knowledge.

In this paper, we present a comprehensive study of the partial decays widths and BR's (including the radiative decay $\tilde{\chi}_2^0 \to \tilde{\chi}_1^0\gamma$ and the decay into a light Higgs boson $\tilde{\chi}_2^0 \to \tilde{\chi}_1^0 h^0$) of the next-to-lightest neutralino in the MSSM. The dependence on all the SUSY parameters is carefully considered, and nontrivial behaviors are found when varying the different parameters.

We assume the usual MSSM framework [1], that is, (1) a minimal content of particles and gauge groups, (2) unification conditions for gauge couplings, gaugino and scalar masses at the grand unified theory (GUT) scale, and (3) R parity is conserved.

We also assume that the lightest neutralino is the LSP.

All masses and couplings are set by choosing the values of a finite set of parameters at the GUT scale: m_0 (the common scalar mass), $m_{1/2}$ (the common gaugino mass), μ (the SUSY Higgs-mixing mass), and $\tan\beta$ (the ratio of vacuum expectation values for the two Higgs doublets). A further parameter, m_{A^0}, is needed to describe the Higgs sector, in case one does not use the constraints coming from the requirement that the radiative electroweak-symmetry breaking takes place at the correct scale.

In Ref. [3], we describe the equations that allow us to get the complete SUSY mass spectrum and couplings starting from the above parameters in a standard approximation. We neglect the possibility of mixing between left and right scalar partners of fermions that can be relevant in the top squark sector, since this has a marginal role in our study. As for the Higgs sector (that is composed by two minimal doublets), we include the leading logarithmic radiative corrections to masses and couplings [8].

The present work complements Ref. [3], where $\tilde{\chi}_1^0\tilde{\chi}_2^0$ production rates and signatures have been studied at the CERN e^+e^- collider LEP 2, by studying extensively the decay features of the $\tilde{\chi}_2^0$ for a wide choice of SUSY parameters. Particular attention is paid to scenarios that are typical of LEP 2 physics.

*Electronic address: ambrosanio@roma1.infn.it
†Electronic address: mele@roma1.infn.it

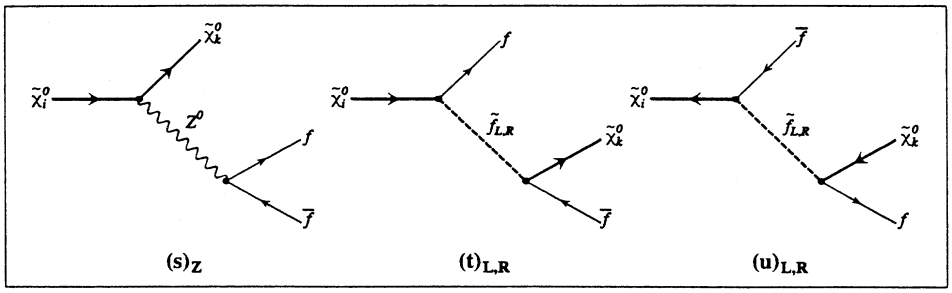

FIG. 1. Feynman diagrams for the three-body neutral decays of the neutralinos.

The plan of the paper is the following. In Sec. II, all the next-to-lightest neutralino decay channels in the MSSM are reviewed. Also, we study contour plots of the neutralino-neutralino and neutralino-chargino mass differences, that are crucial for the analysis of the kinematical features of the decays. In Sec. III, neutralino BR's are presented in the (μ, M_2) plane. In Sec. IV, some specific scenarios that are of interest for LEP 2 neutralino searches, are analyzed. In Sec. V, the hypothesis of a light Higgs boson is considered. Finally, in Sec. VI, the radiative decay $\tilde{\chi}_2^0 \to \tilde{\chi}_1^0\gamma$ is studied.

II. NEUTRALINO-DECAY CLASSIFICATION

In the MSSM, four fermionic partners of the neutral components of the SM electroweak gauge and Higgs bosons are predicted: the photino $\tilde{\gamma}$, the Z-ino $\tilde{Z}$ [mixtures of the U(1) $\tilde{B}$ and SU(2) $\tilde{W}_3$ gauginos], and the two Higgsinos $\tilde{H}_1^0$ and $\tilde{H}_2^0$ (partners of the two Higgs-doublet neutral components). In general, these interaction eigenstates mix, their mixing being controlled by a mass matrix Y (see, e.g., Refs. [3,9,10]). By solving a fourth degree eigenvalue equation, one can find the expressions of $m_{\tilde{\chi}_i^0}$ $(i = 1, \ldots, 4)$ and of the physical composition of the corresponding eigenstates in terms of the set of independent parameters μ, M_2, and $\tan\beta$. Here, we are mainly concerned with the two lightest neutralino states $(i = 1, 2)$. The best direct experimental limits on the $\tilde{\chi}_1^0$ and $\tilde{\chi}_2^0$ masses exclude the ranges $m_{\tilde{\chi}_1^0} < 20\,\text{GeV}$ and $m_{\tilde{\chi}_2^0} < 46\,\text{GeV}$, under the assumption that $\tan\beta > 2$, at LEP 1. These limits disappear if $\tan\beta < 1.6$ [11]. At LEP 2, because of the smaller relative importance of the Z^0-exchange diagram in the $\tilde{\chi}_1^0\tilde{\chi}_2^0$ production, different physical components of neutralinos (and not only Higgsinos) come into play and the common scalar mass m_0 becomes a relevant parameter too. In this framework, in order to put new direct limits on the neutralino masses, one must have a complete knowledge also of the $\tilde{\chi}_2^0$ decay pattern.

In Ref. [3], the behavior of the $\tilde{\chi}_{1,2}^0$ gaugino and Higgsino components is studied in detail in the SUSY parameter space. This is crucial also in understanding the dynamics of the neutralino decays, since different components are coupled to different particles. For instance, in the tree-level decays of neutralinos $\tilde{\chi}_i^0 \to \tilde{\chi}_j^0 f\bar{f}$, there are two main contributions coming from the Z^0 and sfermion exchanges. While the gaugino components couple to the scalars, the Higgsino components couple only to the Z^0 boson, with different strength (in the $m_f = 0$ limit). Also, the neutralino mass spectrum depends on the same three parameters μ, M_2, and $\tan\beta$. A detailed discussion on the $\tilde{\chi}_i^0$ mass spectrum can be found in Refs. [3,10].

In what follows, we list all the possible next-to-lightest neutralino decays in the MSSM. In general, these channels are valid also for heavier neutralinos, although the possibility of cascade decays can make the decay structure of the heavier neutralinos more complicated.

(a) Decay into charged leptons:

$$\tilde{\chi}_2^0 \to \tilde{\chi}_1^0 e^+ e^- , \tag{2.1}$$

or $e^\pm \to \mu^\pm$, $\tau^\pm$.

(b) Decay into a neutrino pair:

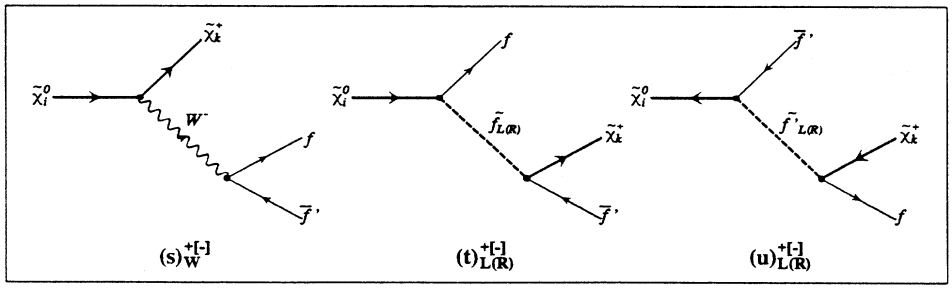

FIG. 2. Feynman diagrams for the three-body charged decays of the neutralinos.

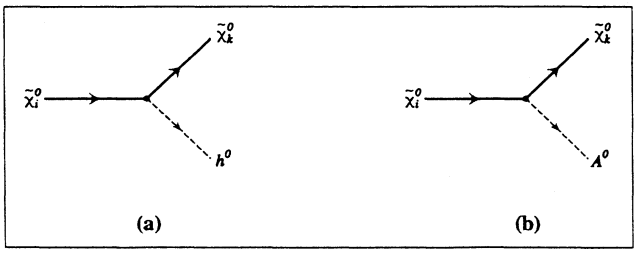

FIG. 3. Feynman diagrams for the neutralino decays in neutral Higgs bosons.

$$\tilde{\chi}_2^0 \to \tilde{\chi}_1^0 \nu_\ell \bar{\nu}_\ell \,, \tag{2.2}$$

where $\ell = e, \mu, \tau$.

(c) Decay into a light-quark pair:

$$\tilde{\chi}_2^0 \to \tilde{\chi}_1^0 q \bar{q} \,, \tag{2.3}$$

where $q = u, d, s, c, b$.

(d) Cascade decay through a real chargino:

$$\begin{aligned} \tilde{\chi}_2^0 \;\to\; & f_1 \bar{f}_1' \, \tilde{\chi}_1^\pm \\ & \hookrightarrow f_2 \bar{f}_2' \tilde{\chi}_1^0 \,, \end{aligned} \tag{2.4}$$

where each pair of fermions $f_i f_i'$ in the final state is an isospin doublet of either leptons or light quarks.

(e) Decay into a light scalar (h^0) or pseudoscalar (A^0) Higgs boson:

$$\tilde{\chi}_2^0 \to \tilde{\chi}_1^0 h^0 \,, \tag{2.5a}$$

$$\tilde{\chi}_2^0 \to \tilde{\chi}_1^0 A^0 \,, \tag{2.5b}$$

where h^0 and A^0 are parts of the MSSM Higgs doublet.

(f) Radiative decay into a photon:

$$\tilde{\chi}_2^0 \to \tilde{\chi}_1^0 \gamma \,. \tag{2.6}$$

The first three channels occur through either a Z^0 or a scalar-particle exchange. Different scalar partners come into play: (left or right) selectron [in channel (a)], (left) sneutrino [in channel (b)], and (left or right) squark [in channel (c)] (see Fig. 1), massless fermions make the channels proceeding through neutral Higgs bosons vanish in a, b, and c . We name s channels the contributions from diagrams with the two neutralinos entering the same vertex (Z^0 exchange), and (t, u) channels the ones where the two neutralinos enter different vertices (sfermion exchange).

Whenever the $\tilde{\chi}_2^0$ is heavier than some scalar fermions, the corresponding channels will proceed through two steps via real sparticles.

A possible gluino in the final state ($\tilde{\chi}_2^0 \to \tilde{g} q \bar{q}$) is excluded by the gaugino mass unification hypothesis, that makes gluinos considerably heavier than light neutralinos.

Cascade decays through a real chargino (d) occur via similar graphs (Fig. 2). The diagrams for the second-step decay [cf. Eq. (2.4)] can be obtained by the same graphs by exchanging the neutralino and the chargino.

As for the channel (e), there are five possible Higgs bosons (either neutral or charged) that could contribute to the tree-level $\tilde{\chi}_2^0$ decays into a scalar Higgs boson plus a light neutralino or chargino. For the next-to-lightest neutralino, only decays into the two lightest bosons (i.e., the lightest neutral scalar and the pseudoscalar Higgs bosons) can be present for the moderate $\tilde{\chi}_2^0$ masses we

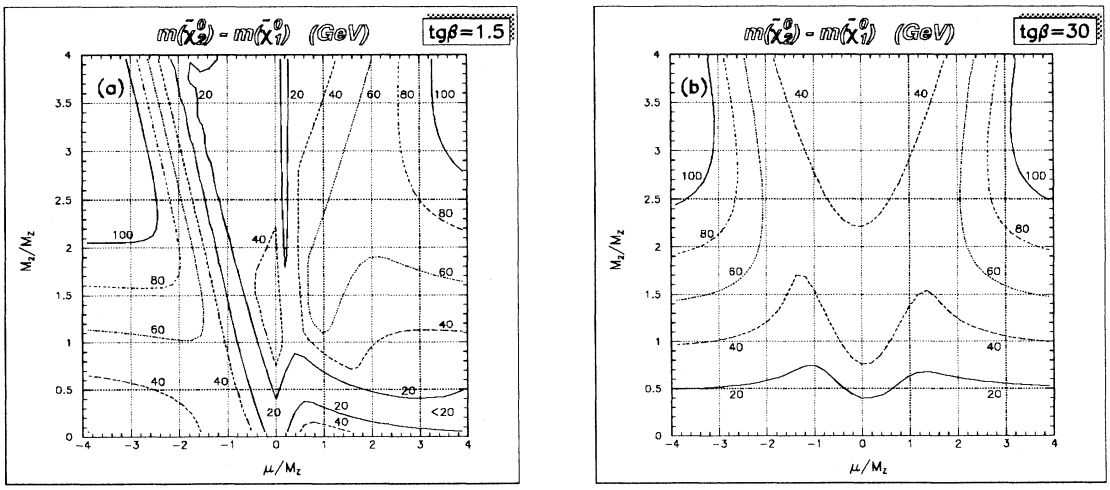

FIG. 4. Contour plot in the (μ, M_2) plane for the difference between the two lightest neutralino masses, for $\tan\beta = 1.5$ (a) and 30 (b).

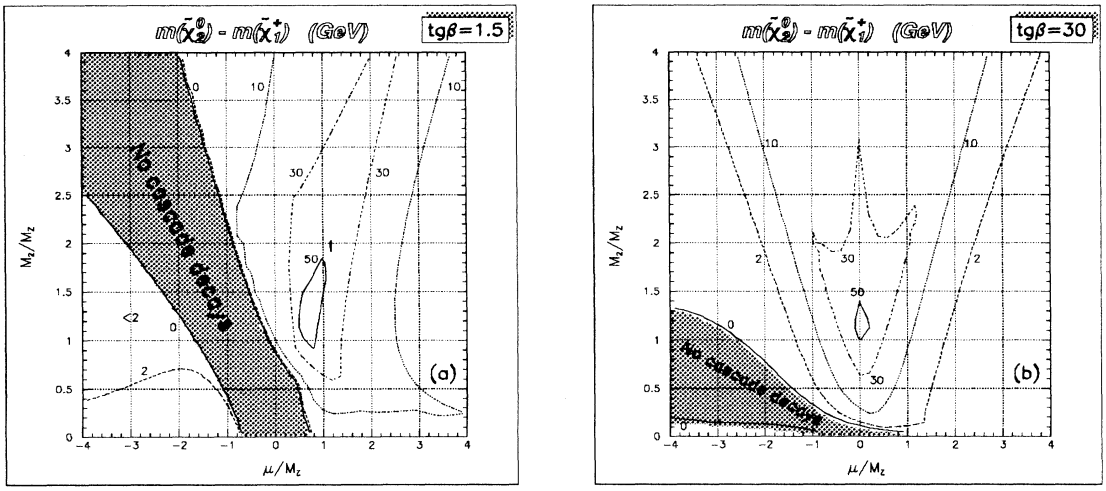

FIG. 5. Contour plot in the (μ, M_2) plane for the difference between the next-to-lightest neutralino mass and the light chargino mass, for $\tan\beta = 1.5$ (a) and 30 (b).

are considering here (Fig. 3).

One important point to keep in mind in the decay study is that, whenever the $\tilde{\chi}_2^0$ can decay into a real scalar plus a fermion (e.g., a selectron plus an electron or a Higgs boson plus a lightest neutralino), this channel tends to saturate the corresponding width and BR. The same occurs when the mass difference between the two lightest neutralinos is sufficient to allow the decay into a real Z^0. In the latter case, the relevant BR's for different signatures recover the Z^0 ones. However, the last possibility never occurs in the LEP 2 parameter regions.

We point out that, apart from the decays into Higgs bosons, that are considered only if the two-body on-shell decay is allowed by the phase space, our treatment of the three-body decays always properly takes into account the possibility of decays into two real particles, whenever this is permitted.

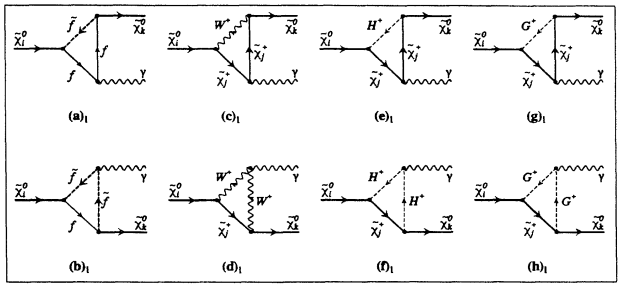

FIG. 6. Feynman diagrams for the radiative neutralino decay $\tilde{\chi}_2^0 \to \tilde{\chi}_1^0\gamma$ in the gauge of Ref. [7]. For each graph shown, there is a further one with clockwise circulating particles in the loop.

In Fig. 4, we show the contour plot for the mass difference between $\tilde{\chi}_2^0$ and $\tilde{\chi}_1^0$, for $\tan\beta = 1.5$ and 30, in the (μ, M_2) plane. From these plots, one can immediately infer, for a given scalar mass, which are the parameter regions where the decays into real scalars are kinematically allowed, and consequently can dominate the $\tilde{\chi}_2^0$ decay.

Furthermore, in Fig. 5, the difference between $m_{\tilde{\chi}_2^0}$ and $m_{\tilde{\chi}_1^\pm}$ is plotted. Shaded areas represent situations where this difference is negative and the neutralino cascade decays through a chargino are not allowed. For small $\tan\beta$, one can anticipate a sizable BR for cascade decays in the positive μ half-plane (cf. Sec. III).

Diagrams contributing to the radiative decay $\tilde{\chi}_2^0 \to \tilde{\chi}_1^0\gamma$ are shown in Fig. 6, where the corresponding graphs with clockwise circulating particles in the loops must be added. The fields $G^\pm$ are the Goldstone quanta giving masses to charged vector bosons. We assume the nonlinear R gauge, that is described in Ref. [7]. One can see that there are many physical charged particles flowing in the loops: all charged standard fermions and their corresponding scalar partners, the charged vector and Higgs bosons, and their fermionic partners, the charginos. In the SUSY parameter scheme we adopt, relevant contributions come mostly from the $W^\pm$ chargino and the top quark–top squark loops, with non-negligible interferences. In this decay, the visible part of the final state is given by a monochromatic photon. From Fig. 4, one can get information on the final photon energy.

In the following analysis, we mainly concentrate on the MSSM parameter regions not excluded at LEP 1. Particular attention is given to regions explorable at the forthcoming experiments, especially at LEP 2 (shown in Fig. 7).

For definiteness, we restrict to the following ranges of SUSY parameters:

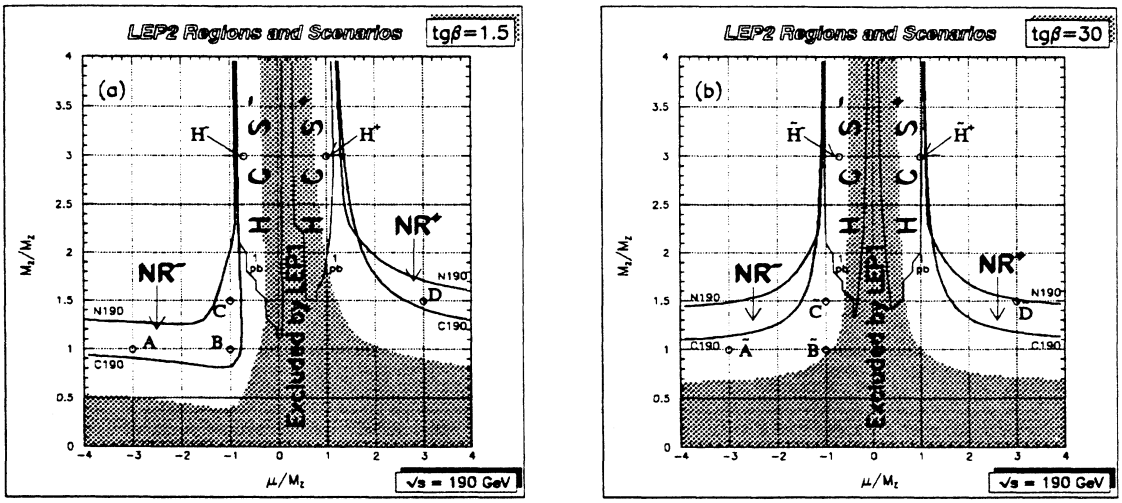

FIG. 7. Interesting regions and scenarios in the (μ, M_2) plane with $\tan\beta = 1.5$ (a) and 30 (b) for neutralino search at LEP 2 ($\sqrt{s} = 190\,\text{GeV}$). The $\text{NR}^{\pm}$ regions (bounded by kinematic-limit curves "N190" and "C190" for $\tilde{\chi}_1^0\tilde{\chi}_2^0$ and $\tilde{\chi}_1^+\tilde{\chi}_1^-$ production, respectively) and $\text{HCS}^{\pm}$ regions (outlined by the 1 pb contour plot for the $\tilde{\chi}_1^0\tilde{\chi}_2^0$ total cross section, for $m_0 = 3M_Z$) are indicated. The shaded area corresponds to LEP 1 limits.

$$0 \leq M_2 \leq 4M_Z, \tag{2.7a}$$

$$-4M_Z \leq \mu \leq 4M_Z, \tag{2.7b}$$

$$40\,\text{GeV} \leq m_0 \leq 500\,\text{GeV}, \tag{2.7c}$$

$$1 < \tan\beta \leq 60, \tag{2.7d}$$

$$M_Z \leq m_{A^0} \leq 3M_Z. \tag{2.7e}$$

The lower limit on m_0 is connected to present experimental limits on the masses of the SUSY partners of leptons and quarks. It generally excludes scenarios where the LSP is a scalar.

III. STUDY OF THE $\tilde{\chi}_2^0$ BR'S IN THE (μ, M_2) PLANE

In this section, we make a detailed study of the BR's for the decay channels (a)–(e) (defined in the previous section) in the (μ, M_2) plane, at fixed values of m_0 and $\tan\beta$. We assume $m_{A^0} = 3M_Z$ that, unless $\tan\beta$ is near 1, generally implies a h^0 mass above the threshold for the channel $\tilde{\chi}_2^0 \to \tilde{\chi}_1^0 h^0$, in the (μ, M_2) region covered by LEP 2 searches. The light-Higgs boson case will be considered in Sec. V, while in Sec. VI we will concentrate on the radiative decay $\tilde{\chi}_2^0 \to \tilde{\chi}_1^0\gamma$. Everywhere the widths and BR's connected to the decays into charged leptons are relative to a single species, while the decays into neutrinos are summed over three families and the decays into quarks over five light flavors. Analogously, for cascade decays, the BR for the leptonic channel is for one single species, while the hadronic channels are summed over two light quark doublets. At this stage, the second-step decay of the $\tilde{\chi}_1^{\pm}$ is not considered.

The BR's for each channel are studied in the (μ, M_2) plane for four different choices of the m_0 and $\tan\beta$ parameters: namely,

$$\text{(a)}: \ (m_0, \tan\beta) = (M_Z, 1.5), \tag{3.1a}$$

$$\text{(b)}: \ = (M_Z, 30), \tag{3.1b}$$

$$\text{(c)}: \ = (3M_Z, 1.5), \tag{3.1c}$$

$$\text{(d)}: \ = (3M_Z, 30), \tag{3.1d}$$

for $|\mu| \leq 4M_Z$ and $0 \leq M_2 \leq 4M_Z$. The observed behavior is in general highly nontrivial, because of both the sharp dependence of the neutralino physical composition on μ and M_2 [3] and the corresponding variation in the neutralino mass spectrum (cf. Fig. 4). Also a weak dependence on M_2 comes from the spectrum of the scalar masses that enter the t-channel contributions to the $\tilde{\chi}_2^0$ decay (Fig. 1).

In Fig. 8, we present the BR for the decay $\tilde{\chi}_2^0 \to \tilde{\chi}_1^0 e^+e^-$. In order to get large BR's, in this case, one needs relatively small m_0 values, so that the t-channel contributions get substantial with respect to the Z^0-exchange channel. In this way, one obtains leptonic BR's much larger than the corresponding $B(Z^0 \to \ell^+\ell^-)$. For instance, when $m_0 = M_Z$ [Figs. 8(a), 8(b)], one always gets wide regions of the plane where $B(\tilde{\chi}_1^0 e^+e^-)$ is larger than 25% (that corresponds to a BR $\geq$ 75% when summed over three lepton species). However, when considering the LEP 2 realm (Fig. 7), the relative importance of these regions is reduced, especially for large $\tan\beta$ values. Note that at large $\tan\beta$, the behavior tends to be more symmetric with respect to the line $\mu = 0$ [Figs. 8(b), 8(d)].

In order to guarantee the detectability of the $\tilde{\chi}_1^0 e^+e^-$ final state in ordinary collider experiments, it is also useful to consider a threshold on the minimum energy

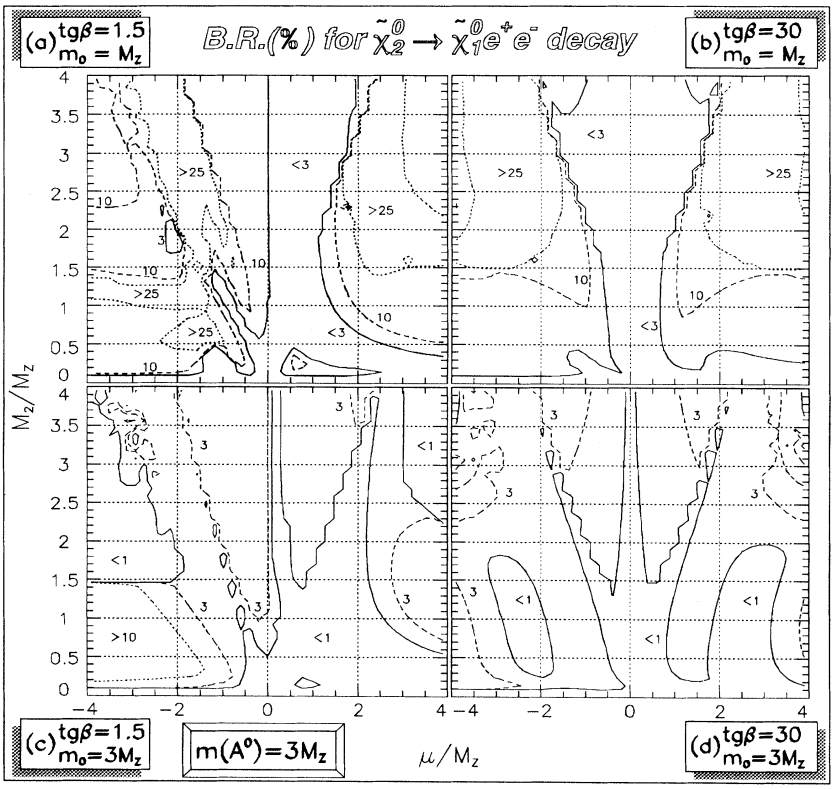

FIG. 8. Contour plot in the (μ, M_2) plane for the BR (%) of the decay $\tilde{\chi}_2^0 \to \tilde{\chi}_1^0 e^+ e^-$. The values of $\tan\beta$ and m_0 are shown in each case [cf. Eqs. (3.1)]. Lines of different style represent contour levels for different values of the BR (as indicated, these values can change case-by-case). All results are obtained assuming $m_{A^0} = 3M_Z$.

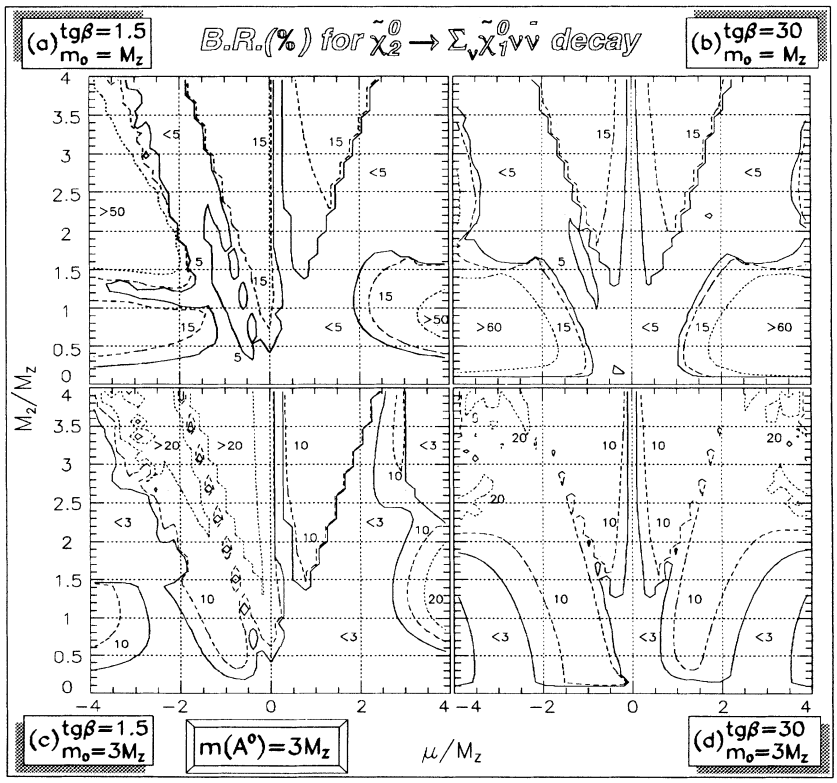

FIG. 9. The same as in Fig. 8, but for the decay $\tilde{\chi}_2^0 \to \sum_\ell \tilde{\chi}_1^0 \nu_\ell \bar{\nu}_\ell$.

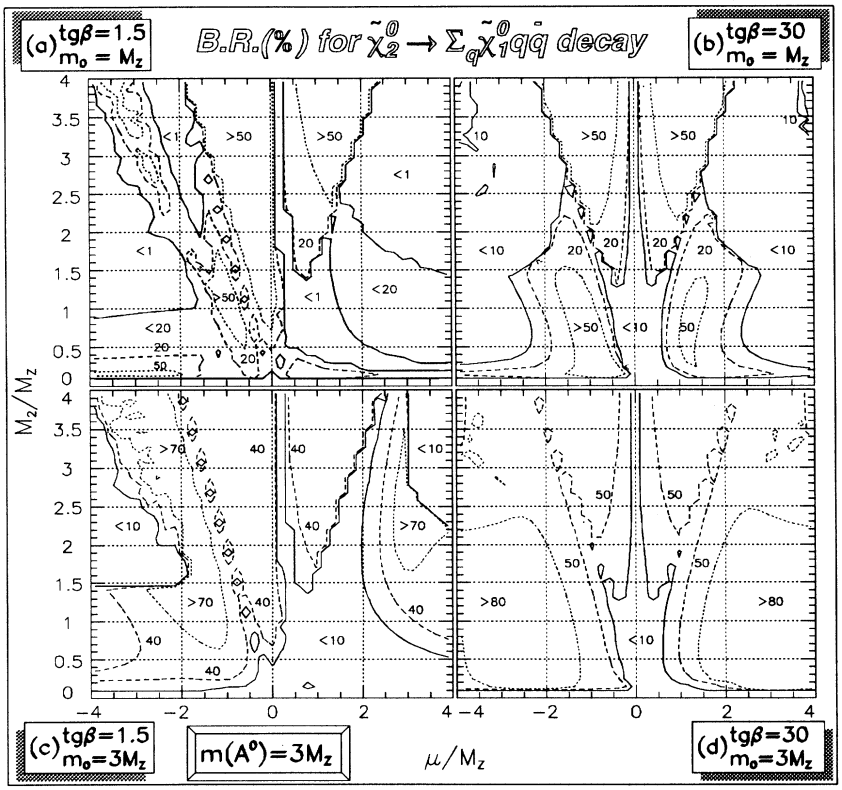

FIG. 10. The same as in Fig. 8, but for the decay $\tilde{\chi}_2^0 \to \sum_q \tilde{\chi}_1^0 q\bar{q}$.

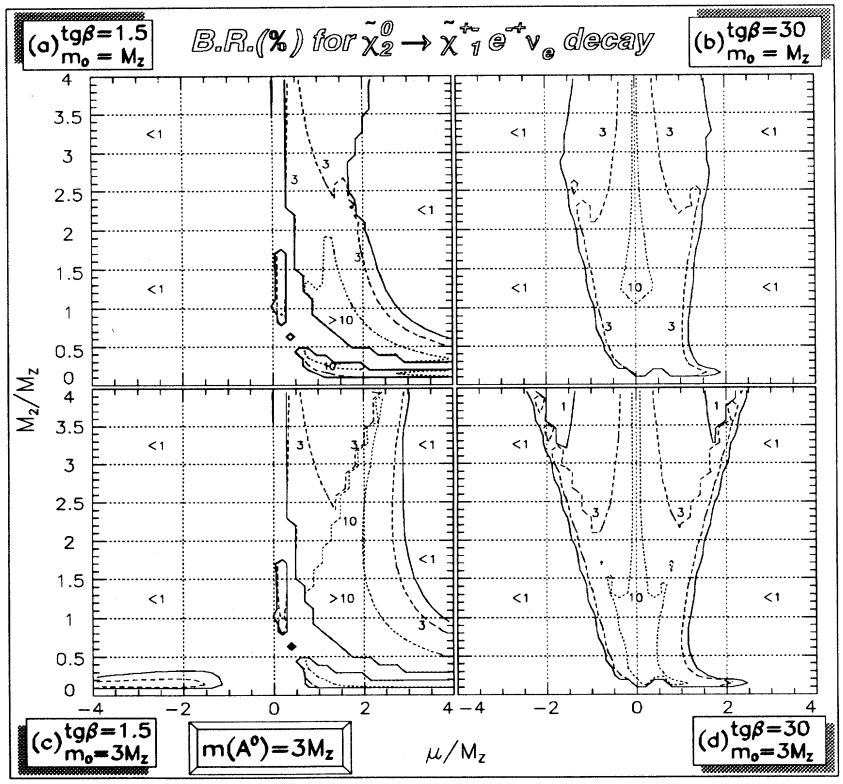

FIG. 11. The same as in Fig. 8, but for the decay $\tilde{\chi}_2^0 \to \tilde{\chi}_1^\pm \ell^\mp \nu_\ell$.

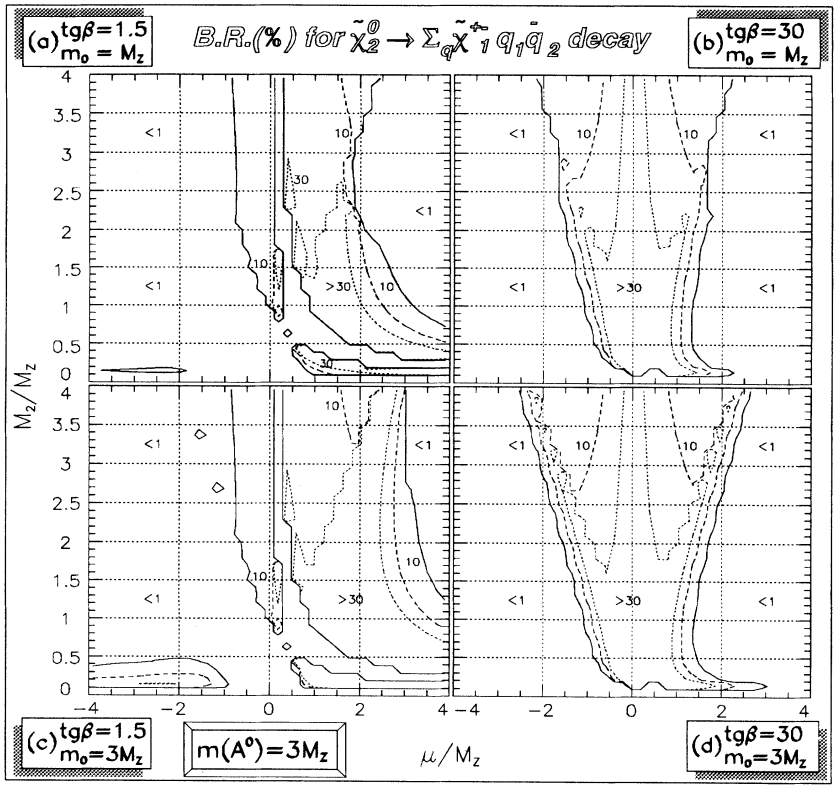

FIG. 12. The same as in Fig. 8, but for the decay $\tilde{\chi}_2^0 \to \sum_q \tilde{\chi}_1^{\pm} q\bar{q}'$.

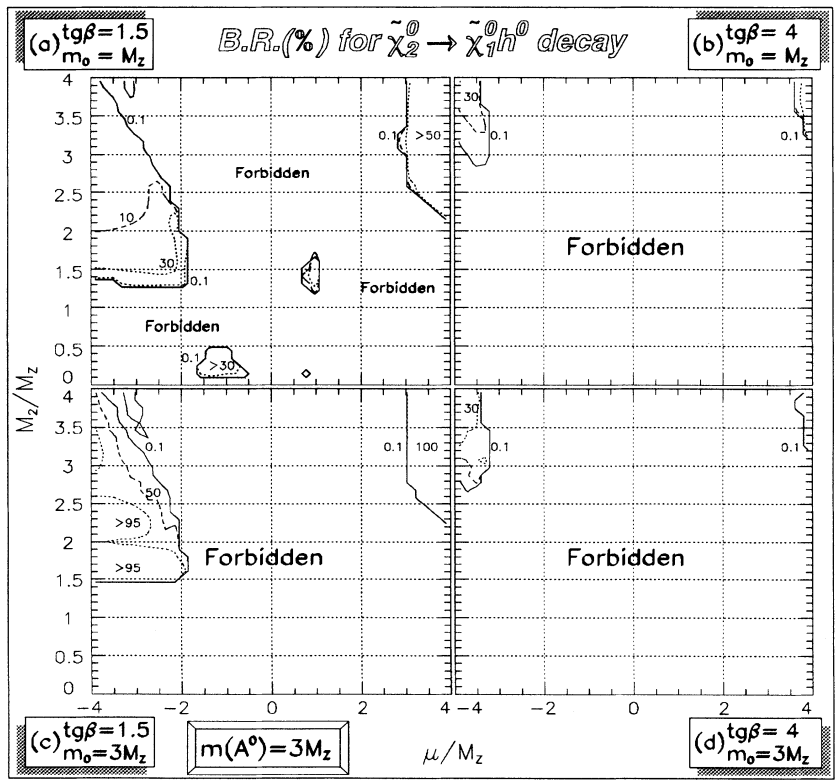

FIG. 13. Contour plots in the (μ, M_2) plane for the BR (%) of the decay $\tilde{\chi}_2^0 \to \tilde{\chi}_1^0 h^0$. The values of $\tan\beta$ and m_0 are shown in each case. All results are obtained assuming $m_{A^0} = 3M_Z$.

for an observable e^+e^- state. The effect of this condition can be guessed through Fig. 4, since $(m_{\tilde{\chi}^0_2} - m_{\tilde{\chi}^0_1})$ is directly connected to the final e^+e^- energy. For instance, one can see that the rejection of the areas where $(m_{\tilde{\chi}^0_2} - m_{\tilde{\chi}^0_1}) < 20\,\text{GeV}$ has a moderate influence on LEP 2 physics (cf. Fig. 7).

In Fig. 8(a), the large BR at moderate values of M_2 and $\mu < 0$ is because of the opening of the tree-level channel $\tilde{\chi}^0_2 \to e^{\mp}\tilde{e}^{\pm}_R$ at $m_0 \approx M_Z$, which is not contrasted by $\tilde{\chi}^0_2 \to \nu_e\tilde{\nu}_{e,L}$ (in general, $m_{\tilde{e}_R} < m_{\tilde{\nu}_{e,L}}$ [3,12]). See Fig. 14 for further details.

In Fig. 9, the channel $\tilde{\chi}^0_2 \to \tilde{\chi}^0_1\nu_\ell\bar{\nu}_\ell$ is studied. As in the previous case, low m_0 values tend to enhance the BR. Note that, in both the charged lepton and the neutrino case, the corresponding Z^0 BR's are recovered in the region of small $|\mu|$ and $M_2 \gtrsim$ (1–2) M_Z. Indeed, in this region, the Higgsino components and, consequently, the Z^0-exchange channels are dominant, independently of m_0 and $\tan\beta$.

This is also true for the hadronic channel that is considered in Fig. 10. On the other hand, in the hadronic decay, a low m_0 value can decrease the BR with respect to the Z^0-channel expectation. This is because, for a given m_0, of the larger value of the squark masses (entering the t-channel contribution), compared to the slepton masses [3,12]. For large m_0, t channels tend to vanish, and the BR for $\tilde{\chi}^0_2 \to \tilde{\chi}^0_1 f\bar{f}$ recovers the $Z^0 \to f\bar{f}$ one.

Cascade decay BR's are shown in Figs. 11 and 12 for the channels $\tilde{\chi}^0_2 \to \tilde{\chi}^{\pm}_1 e^{\mp}\nu_e$ and $\tilde{\chi}^0_2 \to \sum_q \tilde{\chi}^{\pm}_1 q\bar{q}'$, respectively. At small values of $\tan\beta$, the importance of this channel is restricted to the positive-μ half-plane in connection to the regions where $\tilde{\chi}^{\pm}_1$ is sufficiently lighter than $\tilde{\chi}^0_2$ [cf. Figs. 11(a), 11(c), 12(a),12(c) and 5]. The leptonic channel can reach a BR of 10% for each leptonic species at low $\tan\beta$. The relevance of this decay is further increased at larger m_0 [cf. Fig. 11(c)]. Raising $\tan\beta$ makes the pattern symmetrical with respect to the $\mu = 0$ axis, although the BR never reaches a sizable level in the interesting regions [cf. Figs. 11(b), 11(d)]. An analogous situation is observed for the decay into $\tilde{\chi}^{\pm}_1 q\bar{q}'$ in Fig. 12.

In Fig. 13 we study the channel $\tilde{\chi}^0_2 \to \tilde{\chi}^0_1 h^0$. Whenever the light-Higgs-boson mass is lighter than the difference $(m_{\tilde{\chi}^0_2} - m_{\tilde{\chi}^0_1})$, this process has a large BR because of the two-body nature of the decay. The Higgs boson mass spectrum is fixed here by $m_{A^0} = 3M_Z$ that corresponds to m_{h^0} in the range $50 \div 90\,\text{GeV}$, at $\tan\beta = 1.5$ and 100–130 GeV, at $\tan\beta = 30$, for the assumed range of m_0 and M_2.

The most favorable case for the process $\tilde{\chi}^0_2 \to \tilde{\chi}^0_1 h^0$ is the one with small $\tan\beta$ and m_0 [cf. Fig. 13(a)]. Even in this case, the decay threshold opens mostly at relatively large values of $|\mu|$ that correspond to heavier neutralinos. Increasing m_0 [cf. Fig. 13(c)], slightly restricts the allowed regions, because of the $m_{\tilde{t}}$ dependence of the m_{h^0} radiative corrections [8], but, at the same time, increases the branching fraction, because of the depletion of all the other $\tilde{\chi}^0_2 \to \tilde{\chi}^0_1 f\bar{f}$ channels. At $\tan\beta = 30$, the decay $\tilde{\chi}^0_2 \to \tilde{\chi}^0_1 h^0$ is not allowed in almost the whole (μ, M_2) plane considered, because of the increase of m_{h^0} with $\tan\beta$ [8] and also to the decrease of $(m_{\tilde{\chi}^0_2} - m_{\tilde{\chi}^0_1})$ (cf. Fig. 4). In Figs.13(b) and 13(d), an intermediate-$\tan\beta$ situation is shown.

Note that the case of a lighter h^0 (or m_{A^0}) can considerably alter the pattern of the $\tilde{\chi}^0_2$ BR's. The case of a lighter Higgs boson will be considered in Sec. V.

IV. NEUTRALINO DECAYS AT LEP 2

In our analysis of the production of $\tilde{\chi}^0_1\tilde{\chi}^0_2$ pairs at LEP 2 in Ref. [3], we have identified particular regions

TABLE I. Interesting scenarios for neutralino production at LEP 2 ($\sqrt{s} \simeq 190$ GeV) in the case $\tan\beta = 1.5$, $m_0 = M_Z$. Mass eigenvalues for charginos and neutralinos are given as well as the sfermion spectrum arising from $m_0 = M_Z$. For light neutralinos, the physical composition is reported as well.

		Scenarios with $\tan\beta = 1.5$					
	Scenario	A	B	C	D	H^-	H^+
	$(\mu, M_2)/M_Z \to$	(−3, 1)	(−1, 1)	(−1, 1.5)	(3, 1.5)	(−0.7, 3)	(1, 3)
	M_1 (GeV) $\to$	45.7	45.7	68.6	68.6	137.2	137.2
$\tilde{\chi}^0_1$	Mass (GeV)	49.5	51.5	73.7	56.0	62.3	44.9
	$(\tilde{\gamma}, \tilde{Z})$ (%)	(88,11)	(91,6)	(76,10)	(47,45)	(0, 1)	(4,20)
	$(\tilde{H}^0_a\ \tilde{H}^0_b)$ (%)	(1,0)	(2,2)	(1,13)	(7,1)	(2, 97)	(70, 5)
$\tilde{\chi}^0_2$	Mass (GeV)	107.0	85.2	89.8	108.2	−89.1	−92.3
	$(\tilde{\gamma}, \tilde{Z})$ (%)	(12,83)	(4,9)	(15,1)	(53,36)	(0, 7)	(0,0)
	$(\tilde{H}^0_a\ ,\ \tilde{H}^0_b)$ (%)	(4,2)	(0,86)	(2,83)	(10,1)	(90,2)	(5,94)
	$\tilde{\chi}^0_3$ Mass (GeV)	275.4	−129.8	−124.5	−274.4	144.9	153.5
	$\tilde{\chi}^0_4$ Mass (GeV)	−294.9	130.0	166.4	315.6	292.6	304.6
	$\tilde{\chi}^{\pm}_1$ Mass (GeV)	106.1	104.7	110.8	−101.5	80.1	−62.6
	$\tilde{\chi}^{\pm}_2$ Mass (GeV)	291.2	136.2	166.2	310.0	292.2	303.5
	$\tilde{e}_L, \tilde{e}_R, \tilde{\nu}_{e,L}$ Mass (GeV)	124, 104, 114		152,115,144		255,160,250	
	$\tilde{u}_L, \tilde{u}_R$ Mass (GeV)	285, 277		408,395		773,746	
	$\tilde{d}_L, \tilde{d}_R$ Mass (GeV)	289,278		411,395		774,743	

and scenarios in the parameter space. These are characterized by specific dynamical and kinematical properties of the light neutralinos. We have defined as $NR^{\pm}$ (*neutralino regions*) the areas of the (μ, M_2) plane where

$$m_{\tilde{\chi}_1^0} + m_{\tilde{\chi}_2^0} < \sqrt{s} < 2m_{\tilde{\chi}_1^{\pm}} , \tag{4.1}$$

at fixed $\tan\beta$, where $\sqrt{s}$ is the c.m. collision energy at LEP 2 ($\sqrt{s} \simeq 190\,\text{GeV}$) (Fig. 7). In this region, chargino pair production is kinematically forbidden, while, for moderate values of scalar masses, the $\tilde{\chi}_1^0\tilde{\chi}_2^0$ production can have sizable cross sections. Of course, neutralino-pair production can also be of help below the neutralino regions, where it complements chargino production. On the other hand, the largest rates for $e^+e^- \to \tilde{\chi}_1^0\tilde{\chi}_2^0$ arise for $|\mu| \lesssim M_Z$ and $M_2 \gtrsim M_Z$ (what we call $HCS^{\pm}$ stands for *high cross section* regions), although, in these zones, chargino production is also allowed. Here, the Higgsino components of $\tilde{\chi}_1^0$ and $\tilde{\chi}_2^0$ are dominant and the main production mechanism is through Z^0 exchange.

In these regions, for $\tan\beta = 1.5$, we have chosen a set of six specific points [shown in Fig. 7(a)] that can schematize the spectrum of possibilities for the neutralino couplings and masses: scenarios A, B, C, and D in the neutralino regions and $H^{\pm}$ in the high cross section regions. In Table I we show the masses and physical components of the two lightest neutralinos and the mass spectrum of charginos and heavier neutralinos, corresponding to these points in the (μ, M_2) plane. Moreover, we show the sfermion spectrum (that also influences the decay properties of neutralinos) corresponding to these cases for $m_0 = M_Z$. A more detailed analysis of the dynamical characteristics of these scenarios can be found in Ref. [3].

In this section, we present a study of the $\tilde{\chi}_2^0$ widths and BR's in these specific cases. Although the values $\tan\beta = 1.5$ (associated to the definition of such scenarios) and $m_0 = M_Z$ correspond to particularly favorable cases for neutralino production rates, we also study the behavior of decay widths and BR's in a large range of $\tan\beta$ and m_0 values. We will call $\tilde{A}$-$\tilde{H}^{\pm}$ the scenarios with the same values of μ and M_2 as A-$H^{\pm}$, but at $\tan\beta \neq 1.5$ [see, e.g., Fig. 7(b), where $\tan\beta = 30$].

If not otherwise specified, we will assume that decays into real Higgs bosons are not kinematically allowed. In this case, there is some influence of the Higgs boson sector only in the radiative channel. Accordingly, the results presented in this section are obtained for $m_{A^0} = 3M_Z$. The effect of varying m_{A^0} will be discussed in Sec. V.

In Figs. 14–19, we present all partial widths and BR's vs m_0 in the scenarios A, B, C, D, H^-, and H^+. In order to understand the general pattern of the decay widths, one must recall the specific ordering of the scalar masses at fixed m_0 which is predicted by the renormalization group equations and unification assumptions. For instance, one always gets: $m_{\tilde{q}_{L,R}} > m_{\tilde{\ell}_{L,R}}$ and $m_{\tilde{f}_L} > m_{\tilde{f}_R}$. When m_0 is sufficiently small so as to allow $\tilde{\chi}_2^0$ decays into one or more real scalars, the largest decay widths are associated with the corresponding channels that, in general, are the leptonic ones. For instance, this occurs

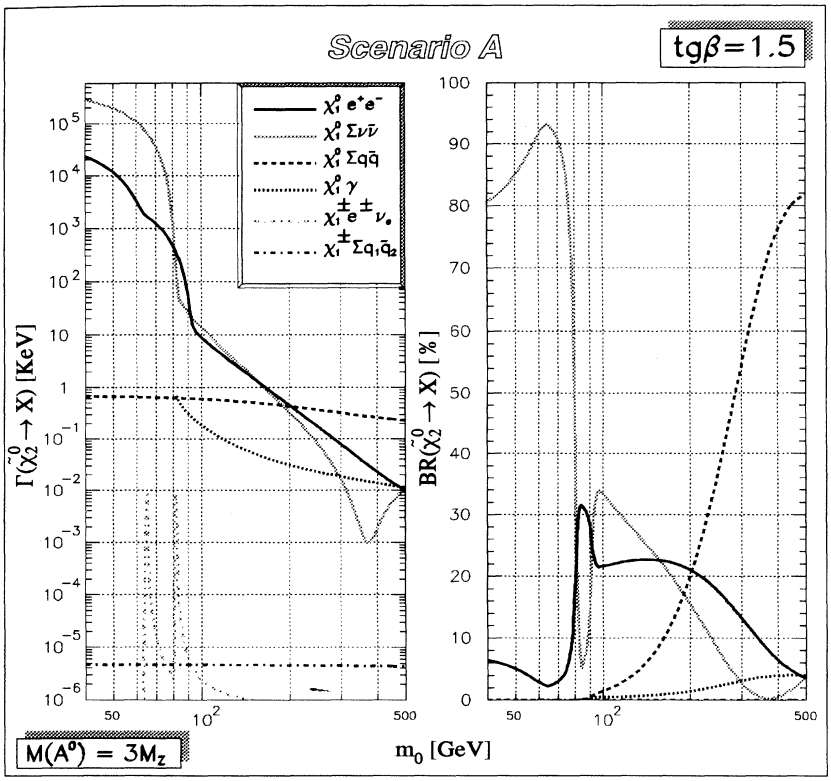

FIG. 14. Widths in keV (left) and BR's in percentage (right) for all the $\tilde{\chi}_2^0$ decays, as functions of the common scalar mass m_0 (GeV), in the scenario A of Table I. The solid, grey, dashed, and dotted lines represent the charged-leptonic, neutrino (summed over three species), hadronic (summed over all light flavors), and radiative channels, respectively. The dot-dashed lines represent the cascade channels. The grey one is for the leptonic case $\tilde{\chi}_2^0 \to \tilde{\chi}_1^{\pm} e^{\mp} \nu_e$, the black one is for the hadronic case $\tilde{\chi}_2^0 \to \sum_q \tilde{\chi}_1^{\pm} q\bar{q}'$, summed over all light flavors. All results are obtained assuming $m_{A^0} = 3M_Z$.

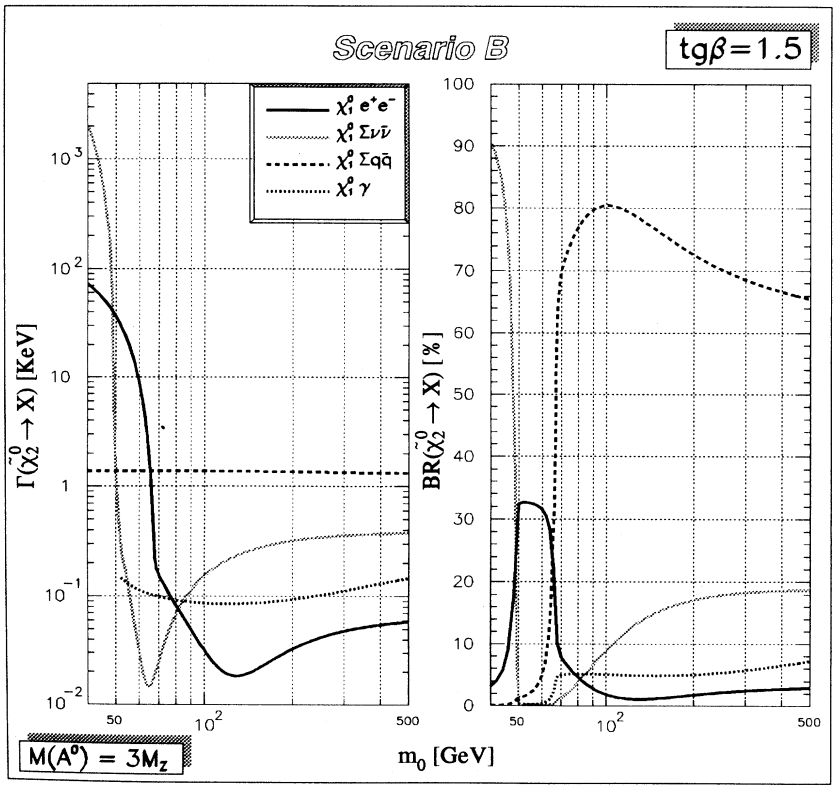

FIG. 15. The same as in Fig. 14, but in the scenario B.

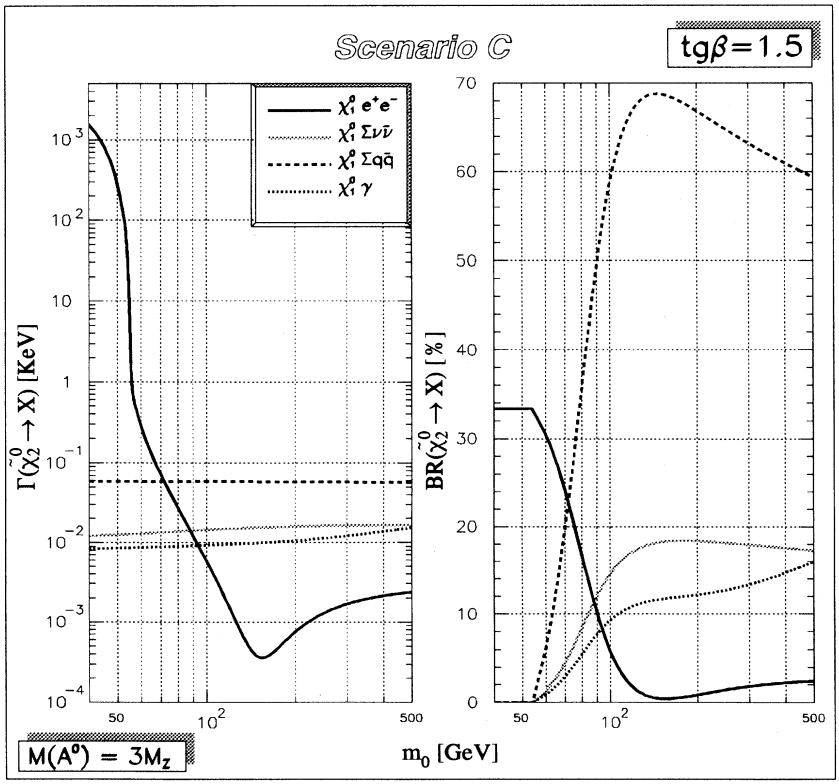

FIG. 16. The same as in Fig. 14, but in the scenario C.

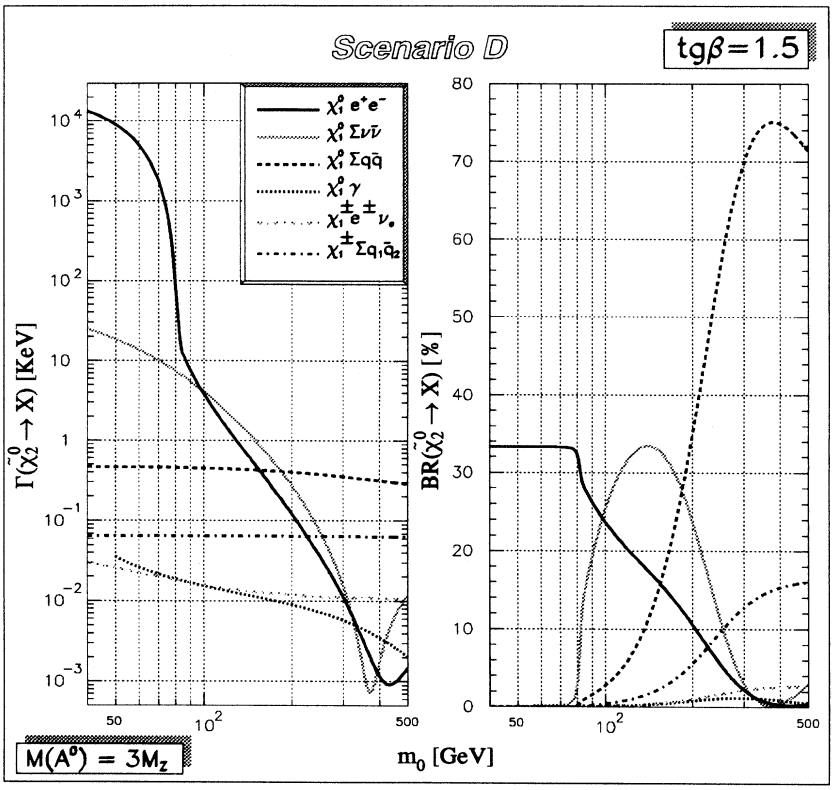

FIG. 17. The same as in Fig. 14, but in the scenario D.

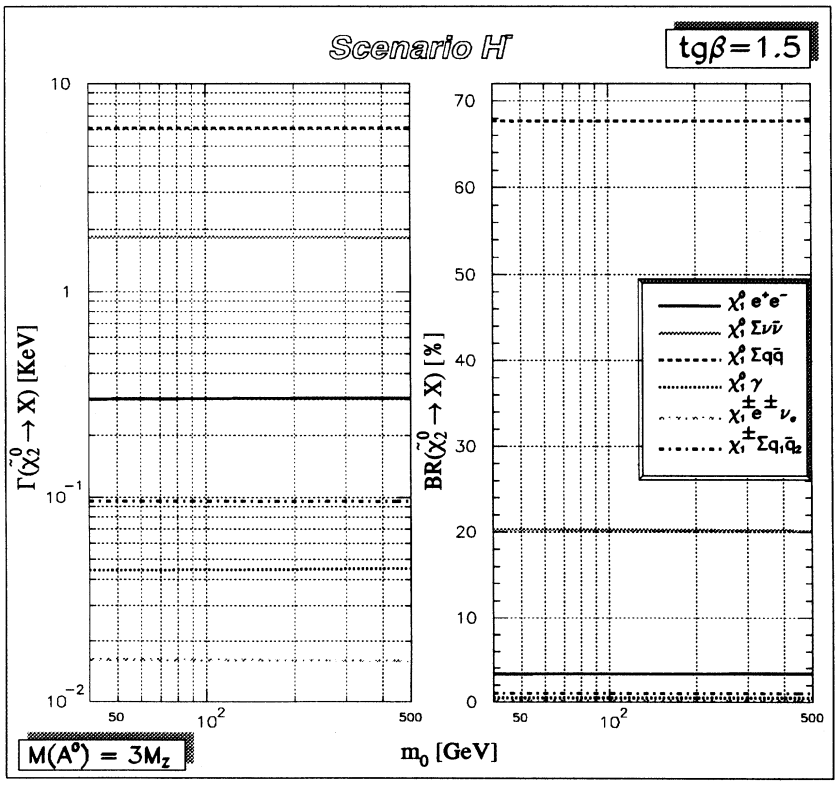

FIG. 18. The same as in Fig. 14, but in the scenario H^-.

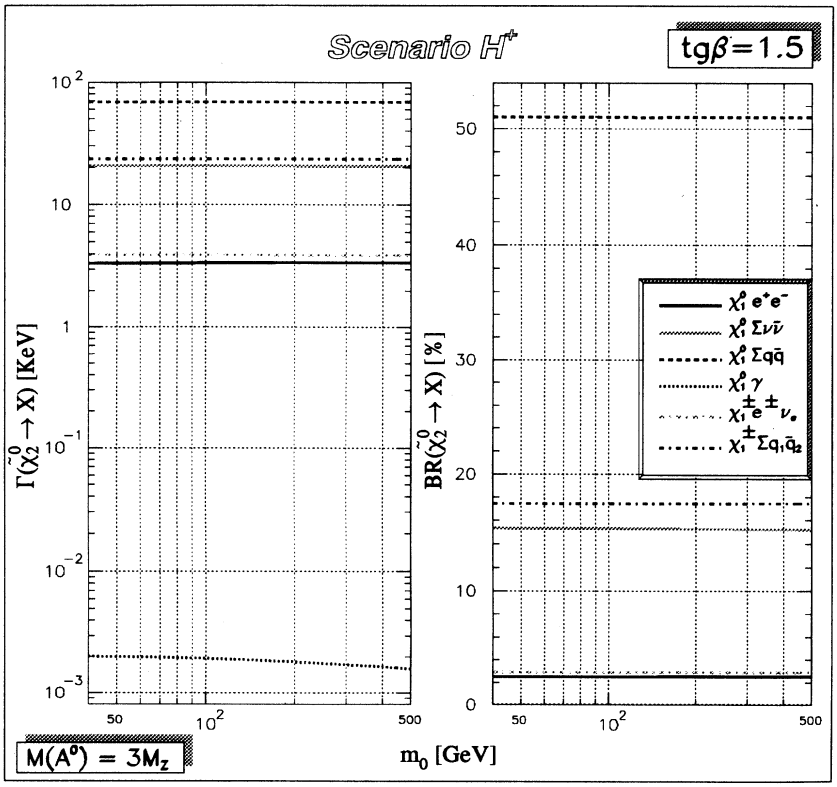

FIG. 19. The same as in Fig. 14, but in the scenario H^+.

for $m_0 \lesssim 100\,\text{GeV}$, in Fig. 14, where we study the scenario A ($\tilde{\chi}^0_{1,2}$ dominantly gauginos, cf. Table I). One can see that the largest rates (up to 1–100 MeV) are by far those corresponding to decays into real sleptons. The width for $\tilde{\chi}^0_2 \to \nu_\ell \bar{\tilde{\nu}}_{\ell,L} \to \nu_\ell \bar{\nu}_\ell \tilde{\chi}^0_1$ is summed over all neutrino flavors, contrary to the charged-lepton channel. For $m_0 \lesssim 60\,\text{GeV}$, all sleptons are produced on the mass-shell. By increasing m_0, one meets, in order, the $m_{\tilde{\ell}_L}$, $m_{\tilde{\nu}_{\ell,L}}$, and $m_{\tilde{\ell}_R}$ thresholds. At large m_0, only the Z^0-exchange contributions survive. Note also the peaks of the leptonic cascade decay width that corresponds to the chain of on-shell decays $\tilde{\chi}^0_2 \to \tilde{e}^\pm_L e^\mp \to \tilde{\chi}^\pm_1 \nu_e e^\mp$ and $\tilde{\chi}^0_2 \to \tilde{\nu}_{e,L}\nu_e \to \tilde{\chi}^\pm_1 e^\mp \nu_e$. When $m_0 \gtrsim 100\,\text{GeV}$, no two-body decay is allowed. On the other hand, in the parameter range considered, one has, in general, $m_{\tilde{q}_{L,R}} > m_{\tilde{\chi}^0_2}$ and the width for the $\tilde{\chi}^0_2 \to q\bar{q}\tilde{\chi}^0_1$ is relatively small and almost constant (between 0.1 and 1 KeV) when varying m_0. Concerning the radiative decay, the curves are obtained through the complete results of Ref. [7]. The width for $\tilde{\chi}^0_2 \to \tilde{\chi}^0_1\gamma$ never exceeds 1 KeV for $m_0 \gtrsim M_Z$.

The corresponding BR pattern closely reflects the scalar-mass threshold structure (Fig. 14). Indeed, for $m_0 \lesssim 75\,\text{GeV}$, the BR for the invisible channel $\tilde{\chi}^0_2 \to \sum_\ell \nu_\ell \bar{\nu}_\ell \tilde{\chi}^0_1$ is more than 80%. Hence, in this regime, the next-to-lightest neutralino is phenomenologically almost equivalent to the LSP, which means that most of the times it just produces missing energy and momentum in the final states. This effect tends to concern even larger ranges of m_0 when $\tan\beta$ increases, because of the relative lowering of the sneutrino mass with respect to the charged-slepton masses. Also, notice that the presence of two close thresholds for the decay into a real $\tilde{\nu}_{\ell,L}$ and a real $\tilde{\ell}_R$ gives rise to a peak structure in the $B(\tilde{\chi}^0_2 \to \ell^+\ell^-\tilde{\chi}^0_1)$ at $m_0 \simeq 83\,\text{GeV}$. This corresponds to a fast deepening in the invisible BR. For $80\,\text{GeV} \lesssim m_0 \lesssim 200\,\text{GeV}$, the largest BR is that for charged leptons ($\gtrsim 60\%$, for all the three lepton species). For $m_0 \gtrsim 200\,\text{GeV}$, the hadronic channel gets more and more important. It reaches 80% for $m_0 \simeq \frac{1}{2}\,\text{TeV}$. The BR for the radiative decay grows with m_0, although at $m_0 \simeq 500\,\text{GeV}$ one still has only BR$\simeq$ 4%. Anyhow, concerning searches at LEP 2, one has to keep in mind that, for $m_0 \gtrsim 300\,\text{GeV}$, the corresponding production rate for $\tilde{\chi}^0_1\tilde{\chi}^0_2$ pairs is below the detectability threshold for a realistic machine luminosity (see Ref. [3]).

In Fig. 15, we deal with the scenario B, where the $\tilde{\chi}^0_1$ is mainly a photino and the $\tilde{\chi}^0_2$ is mainly a $\tilde{H}^0_b$ (cf. Table I). In general, the behavior of widths and BR's is qualitatively similar to the ones in scenario A, apart from the absence of the decay into $\tilde{\ell}_L$ (whose mass is above threshold) and the presence of rather strong destructive interference effects in the leptonic channels. The latter are clearly visible for the process $\tilde{\chi}^0_2 \to \tilde{\chi}^0_1\nu_\ell\bar{\nu}_\ell$ around $m_0 \simeq 64\,\text{GeV}$ and in the case $\tilde{\chi}^0_2 \to \tilde{\chi}^0_1 e^+e^-$ for $m_0 \simeq 130\,\text{GeV}$ (Fig. 15). Indeed, the different physical nature of $\tilde{\chi}^0_1$ and $\tilde{\chi}^0_2$, in particular m_0 ranges, gives rise to a comparable size for the s- and t-channel decay contributions with negative interference of the same order of

magnitude. For instance, in the minimum of the width for the decay into electrons the s channel and t channel contribute 65 and 50 eV, respectively, while their interference give -95 eV.

In the scenario C (cf. Table I) the larger value of M_2 with respect to the previous scenarios generates larger masses in the scalar sector, particularly in the left-handed sector. As a consequence, only the $\tilde{\ell}_R$ can go on mass-shell, while both the invisible and the hadronic widths that are dominated by the Z^0 exchange, keep constant (Fig. 16). As for BR's, the charged-leptonic channels saturate the width up to $m_0 \simeq 64\,\text{GeV}$ (BR$\simeq$ 33% for each lepton species) (Fig. 16). Note that the relatively small widths for the tree-level channels enhance the BR for the radiative decay, for $m_0 \gtrsim 70\,\text{GeV}$, up to about 15%.

The scenario D is chosen in the positive-μ range (contrary to the previous ones) and, in particular, in the area of the neutralino regions where $\tilde{\chi}_2^0$ cascade decays through a light chargino are allowed. The physical composition of $\tilde{\chi}_{1,2}^0$ is given by a mixture of comparable components of $\tilde{\gamma}$ and $\tilde{Z}$ with a small percentage of Higgsino components (cf. Table I). In Fig. 17, the only qualitative new feature in the decay pattern is the presence of sizable widths for cascade decays. The latter are almost constant vs m_0 and give rise to BR's up to 15% for the channel $\tilde{\chi}_2^0 \to \tilde{\chi}_1^\pm q\bar{q}'$ and up to 3% for $\tilde{\chi}_2^0 \to \tilde{\chi}_1^\pm e^\pm \nu_\ell$ at $m_0 \simeq 500\,\text{GeV}$.

In Figs. 18 and 19, we present the $\tilde{\chi}_2^0$ widths and BR's in the High Cross Section regions. In particular, we consider the scenarios $\text{H}^\pm$ defined in Table I. One can check that the Higgsino components in these cases are dominant and the $\tilde{\chi}_1^0$ and $\tilde{\chi}_2^0$ are mostly coupled to the Z^0 boson. Hence, a small dependence on the scalar masses is found. This is the case especially in the H^- scenario (cf. Fig. 18), where the BR for the $q\bar{q}$, $\ell^+\ell^-$, and $\nu_\ell\bar{\nu}_\ell$ channels are quite the same as for Z^0 decays. In Figs. 18 and 19, the widths and BR's for the cascade channels are also reported. The relative importance of these decay modes is considerable only in the H^+ case, where the corresponding BR's reach about 18% for the hadronic mode, and more than 2% for each leptonic channel.

We now proceed to the study of the $\tan\beta$ dependence of the $\tilde{\chi}_2^0$ decay pattern. To this end, as anticipated, we define six new scenarios $\tilde{A}$, $\tilde{B}$, $\tilde{C}$, $\tilde{D}$, $\tilde{H}^\pm$ that are obtained from the above scenarios by fixing $m_0 = M_Z$, and letting free the $\tan\beta$ value. We then study the effect of changing $\tan\beta$ in the range 1–60. Note that, although scenarios A–D were originally defined as lying in the neutralino regions, the variation of $\tan\beta$ can shift such regions above some of these scenarios (cf. Fig. 7). This corresponds to study situations in the (μ, M_2) plane where also chargino production is allowed. Furthermore, changing $\tan\beta$ varies both the mass spectrum and the physical composition of $\tilde{\chi}_{1,2}^0$. For instance, in Fig. 20, the $\tilde{\chi}_2^0$-$\tilde{\chi}_1^0$ and $\tilde{\chi}_2^0$-$\tilde{\chi}_1^\pm$ mass differences (that are crucial quantities entering the phase-space factor of the $\tilde{\chi}_2^0$ widths) are shown vs $\tan\beta$, for the scenarios $\tilde{A}$–$\tilde{H}^+$. Some influence of $\tan\beta$ is also observed in the scalar mass spectrum [3,12].

In Figs. 21–26, the behaviors of $\tilde{\chi}_2^0$ widths and BR's as functions of $\tan\beta$ are shown. In the scenario $\tilde{A}$, we can distinguish three different regimes. For $\tan\beta \leq 1.3$,

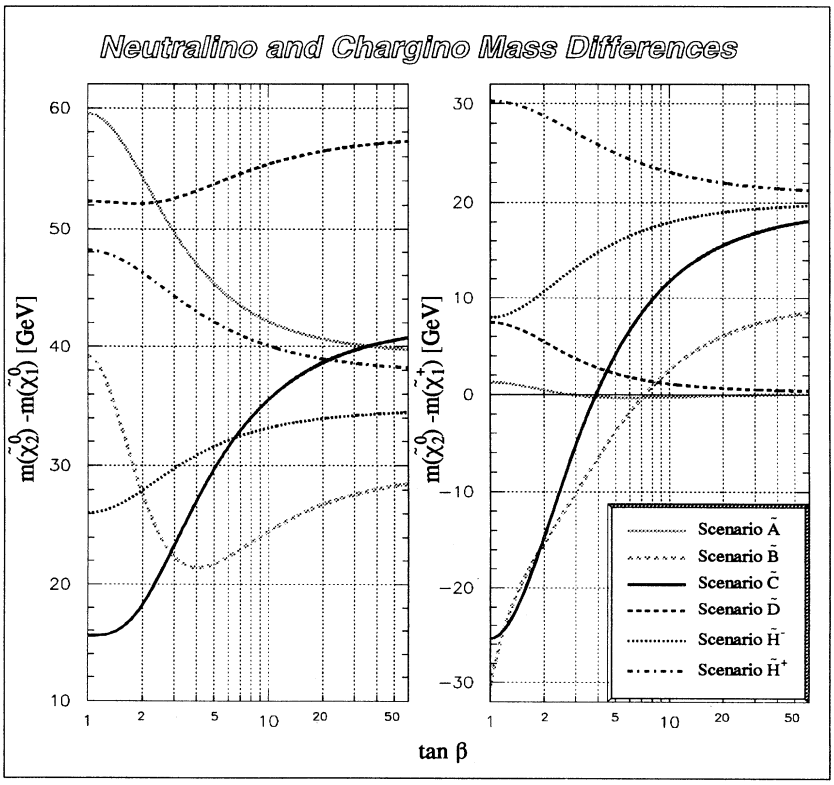

FIG. 20. Difference between the two lightest neutralino masses (left) and between the next-to-lightest neutralino mass and the light chargino mass (right), as functions of $\tan\beta$, in the six scenarios $\tilde{A}$–$\tilde{H}^+$.

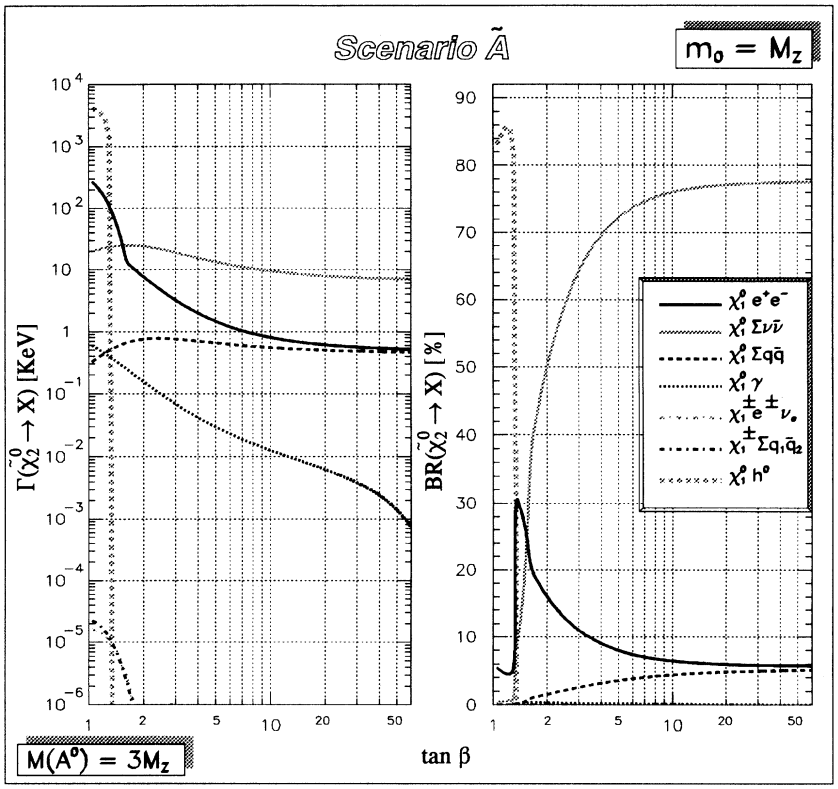

FIG. 21. Widths in keV (left) and BR's in percentage (right) for all the $\tilde{\chi}_2^0$ decays, as functions of $\tan\beta$, in the scenario $\tilde{A}$. The solid, grey, dashed, and dotted lines represent the charged-leptonic, neutrino (summed over three species), hadronic (summed over all light flavors), and radiative channels, respectively. The grey, dashed, thick line is for the channel $\tilde{\chi}_2^0 \to \tilde{\chi}_1^0 h^0$. The dot-dashed lines represent the cascade channels. The grey one is for the leptonic case $\tilde{\chi}_2^0 \to \tilde{\chi}_1^\pm e^\mp \nu_e$, while the black one is for the hadronic case $\tilde{\chi}_2^0 \to \sum_q \tilde{\chi}_1^\pm q\bar{q}'$, summed over all light flavors. All results are obtained assuming $m_{A^0} = 3M_Z$.

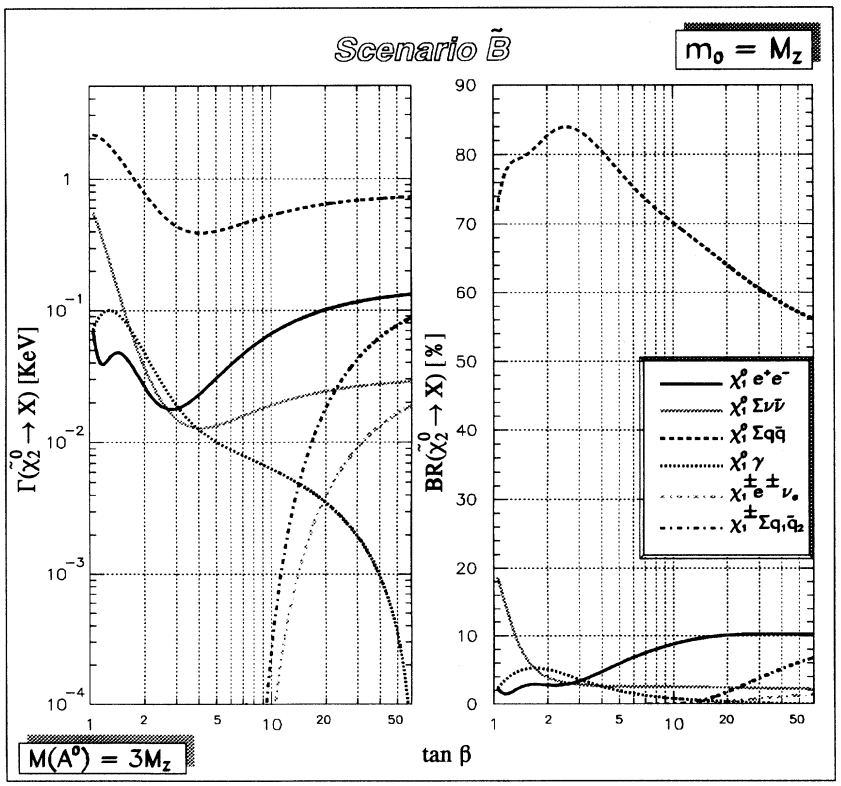

FIG. 22. The same as in Fig. 21, but in the scenario $\tilde{B}$.

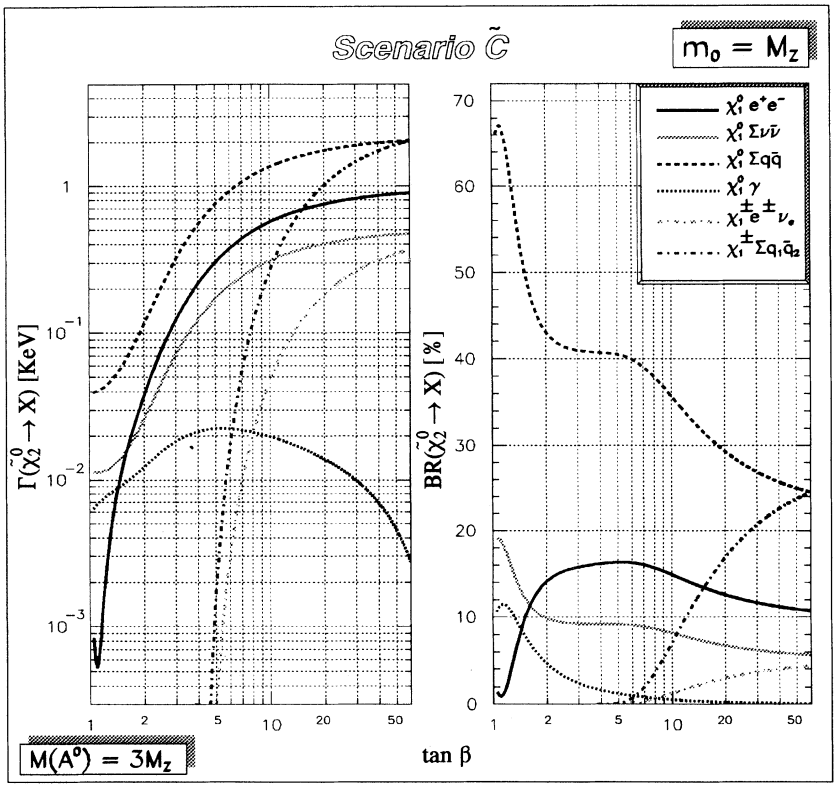

FIG. 23. The same as in Fig. 21, but in the scenario $\tilde{C}$.

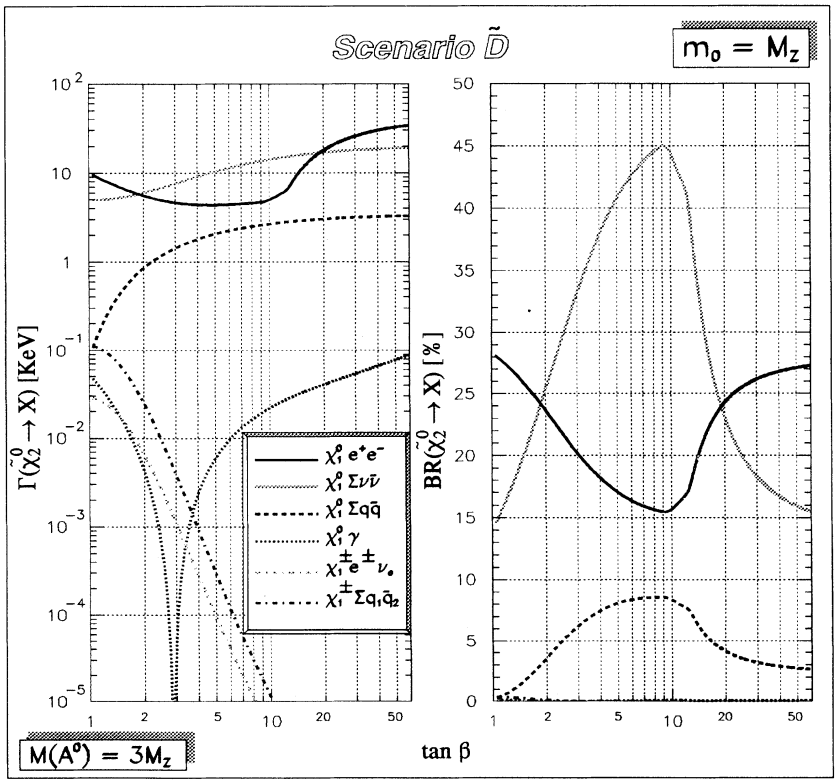

FIG. 24. The same as in Fig. 21, but in the scenario $\tilde{D}$.

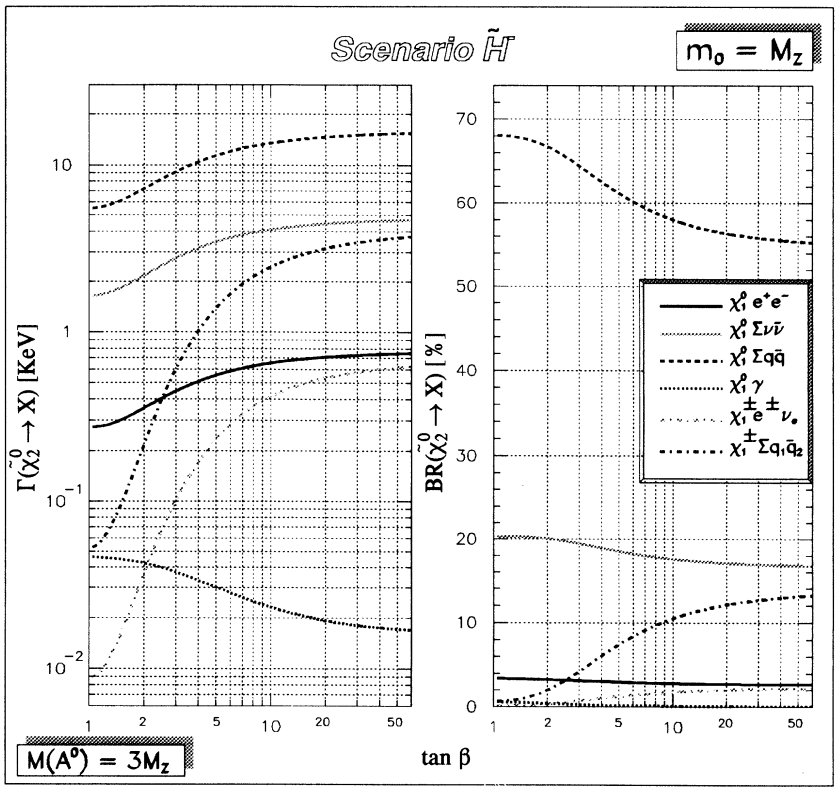

FIG. 25. The same as in Fig. 21, but in the scenario $\tilde{H}^-$.

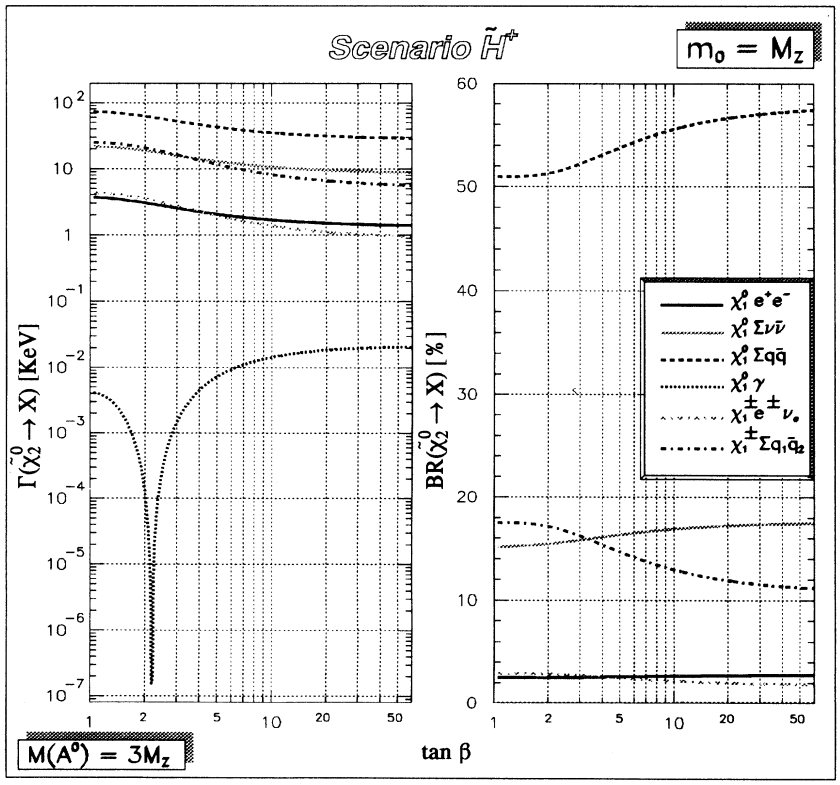

FIG. 26. The same as in Fig. 21, but in the scenario $\tilde{H}^+$.

the tree-level decay into a light Higgs boson h^0 is allowed and the corresponding BR is greater than 80%. Around $\tan\beta = 1.5$, there is a small transition region where the charged-leptonic channel saturates the BR, since the decay into a $\tilde{e}_{L,R}$ is the only possible two-body real channel (this corresponds to the scenario A described above). For larger $\tan\beta$, there is a combined effect of the relative decreasing of the sneutrino mass with respect to the charged slepton masses [3,12] and the increasing Z-ino component in the $\tilde{\chi}_1^0$, that enhances the $\tilde{\chi}_2^0 \to \tilde{\chi}_1^0 \nu_\ell \bar{\nu}_\ell$ decay. Therefore, for large $\tan\beta$ the $\tilde{\chi}_2^0$ gives rise mostly to missing energy and momentum. In the scenario $\tilde{B}$ (Fig. 22), $\tilde{\chi}_2^0 \to \tilde{\chi}_1^0 q\bar{q}$ is dominant in the whole $\tan\beta$ range considered, although the charged-lepton channel has a considerable BR for $\tan\beta \gtrsim 5$–10. In scenario $\tilde{C}$ (Fig. 23), the hadronic channel is the main one for $\tan\beta \lesssim 1.5$–2, while the leptonic channels get comparable to the first at higher $\tan\beta$. Note that, for $\tan\beta \gtrsim 10$, also the cascade decays into a $\tilde{\chi}_1^\pm$ give a sizable contribution.

As for scenario $\tilde{D}$, we note in Fig. 24 a maximum in both the invisible and the hadronic BR's curves corresponding to a deepening of the charged-leptonic one for $\tan\beta \simeq 10$. This is because of the sudden opening of the channel $\tilde{\chi}_2^0 \to e^\pm \tilde{e}_{L,R}^\mp$.

In Figs. 25 and 26, we study the scenarios $\tilde{H}^\mp$. Here, we observe again a BR pattern closely connected to the Z^0 BR's with some deviation because of the possible presence of a light chargino in the cascade decays (see also Fig. 20). In the scenario H^-, the cascade decays contribute considerably at large $\tan\beta$, while in the scenario H^+, they decrease with $\tan\beta$. Note the strong (although not phenomenologically relevant) deepening of the radiative decay width at $\tan\beta \simeq 2.2$, because of destructive interference among various contributions.

V. DECREASING THE HIGGS BOSON MASSES

In this section we study the sensitivity of the $\tilde{\chi}_2^0$ decay widths and BR's to a m_{h^0} change. In particular, we set $m_{A^0} = M_Z$ which, compared to the case $m_{A^0} = 3M_Z$ studied in Sec. III, corresponds to a lowering of m_{h^0} down to 40–70 GeV, at $\tan\beta = 1.5$, and to 90–91 GeV, at $\tan\beta = 30$ in the considered range of m_0 and M_2 (cf. Sec. III).

In Fig. 27(a), we show the $B(\tilde{\chi}_2^0 \to \tilde{\chi}_1^0 h^0)$ when m_{A^0} is lowered down to M_Z. The corresponding reduction of the threshold for the decay $\tilde{\chi}_2^0 \to \tilde{\chi}_1^0 h^0$ considerably extends (with respect to Fig. 13) the area where $B(\tilde{\chi}_1^0 h^0) > 30\%$ in the (μ, M_2) plane, down to regions of interest for LEP 2 physics. In particular, this happens in the regions where the $\tilde{\chi}_{1,2}^0$ gaugino components are large, which implies a considerable decrease in the BR's for all the other decay channels in these regions [as can be checked by comparing Figs. 27(b)–27(d) with Figs. 8(a), 9(a) and 10(a)]. On the contrary, the situation is not altered in the Higgsino region, where $m_{\tilde{\chi}_1^0}$ and $m_{\tilde{\chi}_2^0}$ tend to be degenerate, and the decay $\tilde{\chi}_2^0 \to \tilde{\chi}_1^0 h^0$ is not allowed.

In Figs. 28 and 29, we study the influence of the m_{A^0}

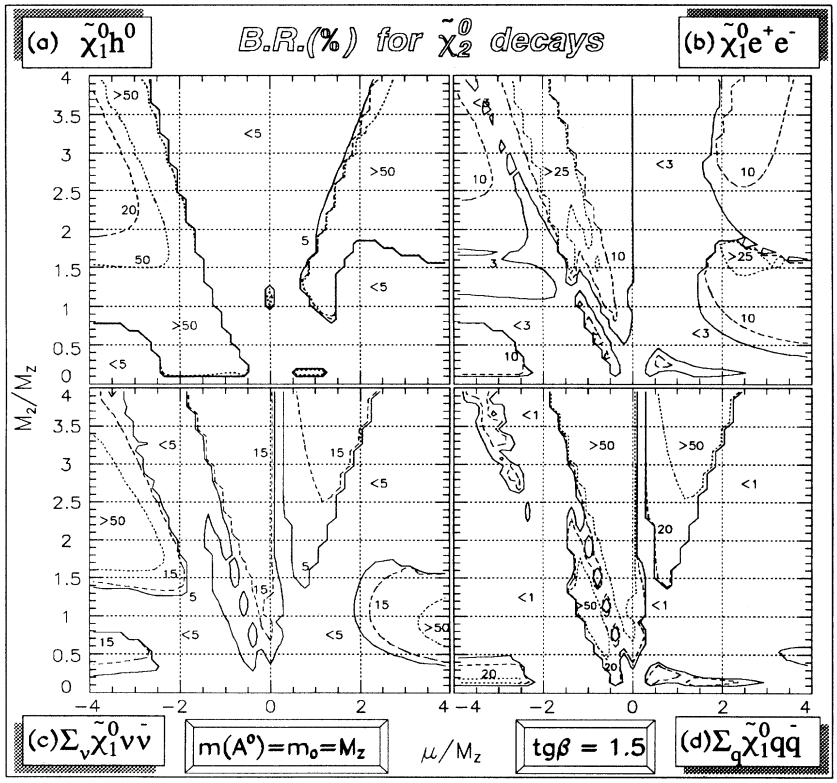

FIG. 27. Contour plot on the (μ, M_2) plane for the BR (%) of the decays: (a): $\tilde{\chi}_2^0 \to \tilde{\chi}_1^0 h^0$, (b): $\tilde{\chi}_1^0 e^+ e^-$, (c): $\sum_\ell \tilde{\chi}_1^0 \nu_\ell \bar{\nu}_\ell$, (d): $\sum_q \tilde{\chi}_1^0 q\bar{q}$ in the case of a light-Higgs boson ($m_{A^0} = M_Z$), for $m_0 = M_Z$ and $\tan\beta = 1.5$.

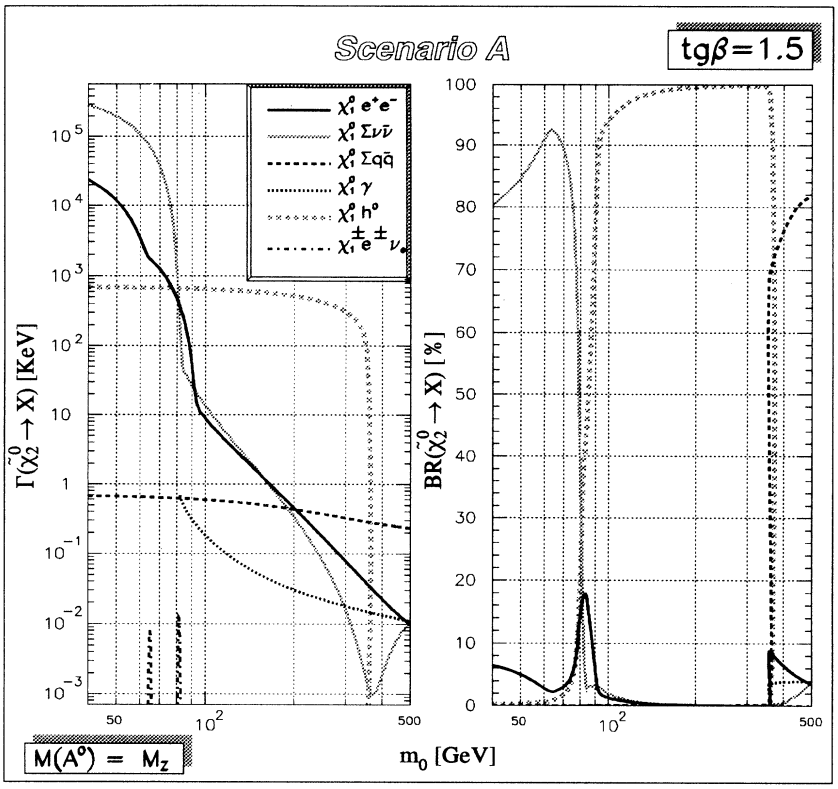

FIG. 28. Widths in keV (left) and BR's in percentage (right) for all $\tilde{\chi}_2^0$ decays, as functions of the common scalar mass m_0 in the scenario A. The solid, grey, dashed, and dotted lines represent the charged-leptonic, neutrino (summed over three species), hadronic (summed over all light flavors), and radiative channels, respectively. The dot-dashed line shows only the peaks of the width for the cascade channel $\tilde{\chi}_2^0 \to \tilde{\chi}_1^\pm e^\mp \nu_e$ (cf. Fig. 14). The grey, dashed, thick line is for the channel $\tilde{\chi}_2^0 \to \tilde{\chi}_1^0 h^0$. All results are obtained assuming $m_{A^0} = M_Z$.

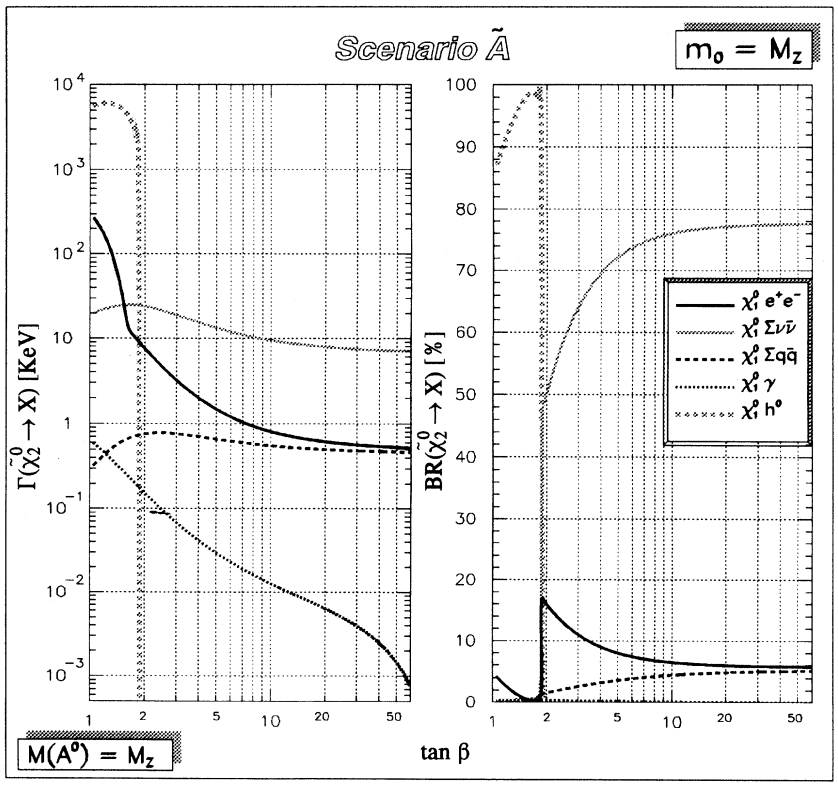

FIG. 29. Widths in keV (left) and BR's in percentage (right) for all the $\tilde{\chi}_2^0$ decays, as functions of $\tan\beta$, in the scenario $\tilde{A}$. All results are obtained assuming $m_{A^0} = M_Z$.

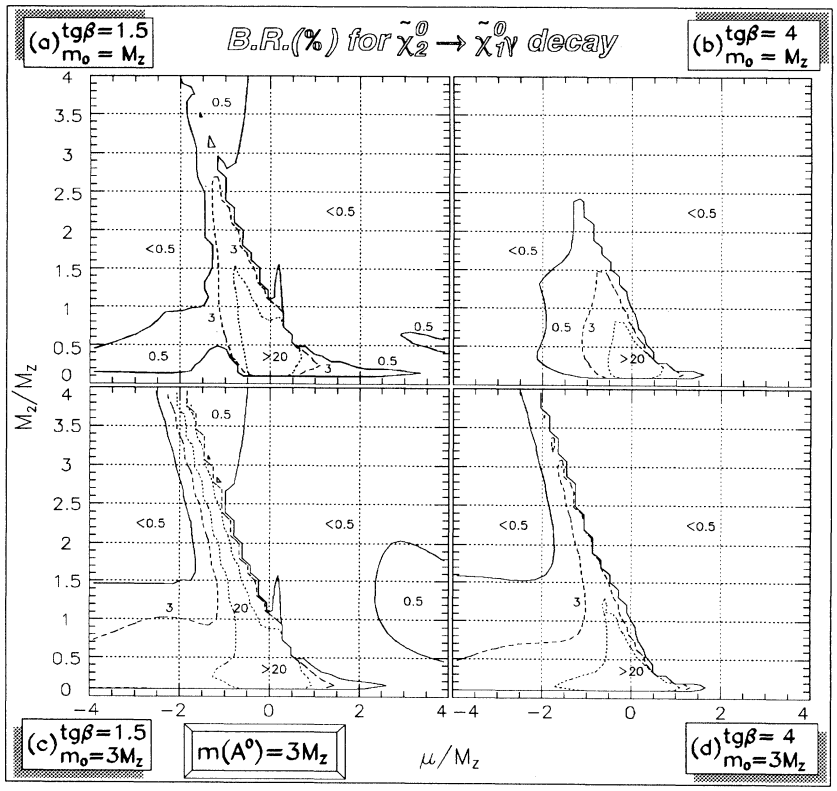

FIG. 30. Contour plot in the (μ, M_2) plane for the BR (%) of the radiative decay $\tilde{\chi}_2^0 \to \tilde{\chi}_1^0\gamma$. The values of $\tan\beta$ and m_0 are shown in each case. All results are obtained assuming $m_{A^0} = 3M_Z$.

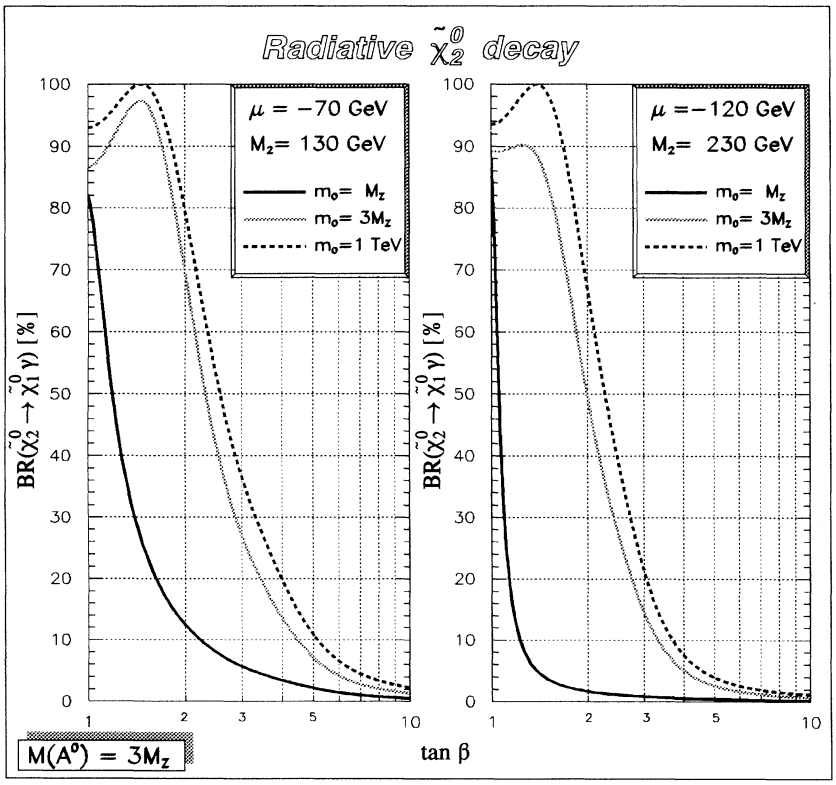

FIG. 31. BR (%) for the radiative decay $\tilde{\chi}_2^0 \to \tilde{\chi}_1^0\gamma$ as function of $\tan\beta$ in the scenarios (i) (left) and (ii) (right) given in the text. In each scenario, the behavior is given for three different values of the common scalar mass: $m_0 = M_Z$ (grey line), $m_0 = 3M_Z$ (solid line), and $m_0 = 1\,\text{TeV}$ (dashed line). All results are obtained assuming $m_{A^0} = 3M_Z$.

decrease in the scenarios $A/\tilde{A}$ considered in Sec. IV. The scenario A is the only one, out of the six defined in Table I, that falls in the area of large $B(\tilde{\chi}_2^0 \to \tilde{\chi}_1^0 h^0)$ for $m_{A^0} = M_Z$. In Fig. 28, one can see the m_0 dependence of widths and BR's (already studied in Fig. 14 for $m_{A^0} = 3M_Z$), when one sets $m_{A^0} = M_Z$. The influence of m_0 on the decay width into a Higgs boson comes from the radiative correction to m_{h^0} through the stop mass [8]. After the low-m_0 range, where the invisible decay $\tilde{\chi}_2^0 \to \tilde{\nu}_{e,L}\nu_e$ is still dominant, we have an intermediate range $M_Z \lesssim m_0 \lesssim 350\,\text{GeV}$, where the $b\bar{b}+\not{E}$ signature (corresponding to the decay into $\tilde{\chi}_1^0 h^0$) is largely dominant. After that, the old pattern of Fig. 14 is recovered with a large hadronic BR from $\tilde{\chi}_2^0 \to \tilde{\chi}_1^0 q\bar{q}$, through the Z^0 exchange. As for the $\tan\beta$ dependence (Fig. 29), the main effect of lowering m_{A^0} with respect to Fig. 21 is an extension of the $\tan\beta$ range where the decay into a light-Higgs boson is relevant, from about (1–1.4) up to about (1–2). Hence, the $\tan\beta$ range where the $\tilde{\chi}_2^0$ decays in something visible is quite widened, in the scenario $\tilde{A}$.

VI. THE RADIATIVE $\tilde{\chi}_2^0$ DECAY

In this section, we study the BR for the decay $\tilde{\chi}_2^0 \to \tilde{\chi}_1^0\gamma$. Provided the mass difference $(m_{\tilde{\chi}_2^0} - m_{\tilde{\chi}_1^0})$ is large enough so as to give rise to a sufficiently energetic photon, this channel can produce a beautiful signature. A monochromatic photon plus missing energy and momentum should be observed. Although in all cases considered in the previous sections, $B(\tilde{\chi}_2^0 \to \tilde{\chi}_1^0\gamma)$ never exceeds 15%, it can reach values as large as 100% in particular regions of the $\mu, M_2, \tan\beta$ space, as we are going to show.

In Fig. 30, the $B(\tilde{\chi}_2^0 \to \tilde{\chi}_1^0\gamma)$ in the (μ, M_2) plane at fixed m_0 and $\tan\beta$ is studied. We will assume $m_{A^0} = 3M_Z$ everywhere. Indeed, although m_{A^0} sets the mass of the charged Higgs boson that flows in the virtual loops (cf. Fig. 6), this parameter is less critical in this study. We have checked that varying m_{A^0} in the range $(M_Z, 1\,\text{TeV})$ can change $B(\tilde{\chi}_2^0 \to \tilde{\chi}_1^0\gamma)$ by at most $\pm 10\%$ (with increasing BR when m_{A^0} grows). The scenarios studied in Fig. 30 assume either $\tan\beta = 1.5$ or 4. The BR for the radiative channel decreases substantially at larger $\tan\beta$. Furthermore, we set either $m_0 = M_Z$ or $3M_Z$, as in the previous sections. One can distinguish a specific area where $B(\tilde{\chi}_2^0 \to \tilde{\chi}_1^0\gamma)$ is large, which, particularly for large m_0 values [cf. Fig. 30(c) and 30(d)], it evolves roughly around the $M_2 = -2\mu$ line. This corresponds to the region where $\tilde{\chi}_1^0$ is a pure Higgsino B, while $\tilde{\chi}_2^0$ is mostly a photino (cf., e.g., Figs. 2.2 and 2.3 in Ref. [3]). This situation hinders all the tree-level decays, since the scalar-exchange decays require gaugino components in both $\tilde{\chi}_1^0$ and $\tilde{\chi}_2^0$, while the Z^0-exchange ones need Higgsino components. By the way, the different gaugino/Higgsino nature of the two lightest neutralinos also depletes the $\tilde{\chi}_1^0\tilde{\chi}_2^0$ pair production in e^+e^- collisions. In Fig. 30, also note that a large fraction of the high-BR region lies in the area excluded by LEP 1 searches. Nevertheless, one can single out particular situations (of interest for LEP 2 physics and even beyond), where one can have very large BR's for the radiative channel.

For instance, in Fig. 31, we study two different scenarios versus $\tan\beta$: (i) $\mu = -70\,\text{GeV}$, $M_2 = 130\,\text{GeV}$, $m_0 = M_Z, 3M_Z, 1\,\text{TeV}$; (ii) $\mu = -120\,\text{GeV}$, $M_2 = 230\,\text{GeV}$, $m_0 = M_Z, 3M_Z, 1\,\text{TeV}$. The scenario (i) is of interest for LEP 2 searches. For instance, for $\tan\beta = 1.5$, one has $m_{\tilde{\chi}_1^0} \simeq 65\,\text{GeV}$ and $m_{\tilde{\chi}_2^0} \simeq 75\,\text{GeV}$. The scenario (ii) concerns heavier neutralino states: for $\tan\beta = 1.5$, one gets $m_{\tilde{\chi}_1^0} \simeq 113\,\text{GeV}$ and $m_{\tilde{\chi}_2^0} \simeq 127\,\text{GeV}$.

Figure 30 shows that $B(\tilde{\chi}_2^0 \to \tilde{\chi}_1^0\gamma)$ is particularly large at moderate $\tan\beta$, although the total width can be as low as a few 10^{-3} eV. The BR is enhanced by increasing m_0, since this makes all the other decay widths decrease further.

On the other hand, one can check that, at $\tan\beta = 1$, $\tilde{\chi}_1^0$ and $\tilde{\chi}_2^0$ are almost degenerate, while their mass difference grows monotonically with $\tan\beta$. In order to have a sufficiently energetic photon, e.g., $E_\gamma \geq 10\,\text{GeV}$, one should restrict to $\tan\beta \gtrsim 1.5$ in the case (i) and to $\tan\beta \gtrsim 1.35$ in the case (ii), which imply $(m_{\tilde{\chi}_2^0} - m_{\tilde{\chi}_1^0}) \gtrsim 10\,\text{GeV}$.

A more in-depth study of the case of large radiative BR will be carried out in a forthcoming paper [13].

ACKNOWLEDGMENT

We thank Guido Altarelli for constant encouragement and discussions.

[1] H. E. Haber and G. L. Kane, Phys. Rep. **117**, 75 (1985).
[2] A. Bartl, H. Fraas, W. Majerotto, and B. Mösslacher, Z. Phys. C **55**, 257 (1992).
[3] S. Ambrosanio and B. Mele, Phys. Rev. D **52**, 3900 (1995).
[4] A. Bartl, H. Fraas, and W. Majerotto, Nucl. Phys. **B278**, 1 (1986); Z. Phys. C **41**, 475 (1988).
[5] J. F. Gunion, *et al.*, Int. J. Mod. Phys. A **4**, 1145 (1987); J .F. Gunion and H. E. Haber, Phys. Rev. D **37**, 2515 (1988).
[6] H. Komatsu and J. Kubo, Phys. Lett. **157B**, 90 (1985); Nucl. Phys. **B263**, 265 (1986); H. E. Haber, G. L. Kane, and M. Quirós, Phys. Lett. **160B**, 297 (1985); Nucl. Phys. **B273**, 333 (1986).
[7] H. E. Haber and D. Wyler, Nucl. Phys. **B323**, 267 (1989).
[8] H. E. Haber and R. Hempfling, Phys. Rev. Lett. **66**, 1815 (1991); Y. Okada, M. Yamaguchi, and T. Yanagida, Prog. Theor. Phys. **85**, 1 (1991); Phys. Lett. B **262**, 54 (1991); J. Ellis, G. Ridolfi, and F. Zwirner, *ibid.* **257**, 83 (1991); **262**, 477 (1991); R. Barbieri, M. Frigeni, and F. Caravaglios, *ibid.* **258**, 167 (1991); A. Yamada, *ibid.*

263, 233 (1991).
[9] J. Ellis and G. G. Ross, Phys. Lett. **117B**, 397 (1982); J. M. Frère and G. L. Kane, Nucl. Phys. **B223**, 331 (1983).
[10] A. Bartl, H. Fraas, W. Majerotto, and N. Oshimo, Phys. Rev. D **40**, 1594 (1989).
[11] L3 Collaboration, M. Acciarri *et al.*, Phys. Lett. B **350**, 109 (1995).
[12] L. E. Ibáñez and C. López, Nucl. Phys. **B233**, 511 (1984); L. E. Ibáñez, C. López, and C. Muñoz, *ibid.* **B256**, 218 (1985); L. E. Ibáñez and G. G. Ross, in "Perspectives on Higgs Physics," edited by G. L. Kane, (World Scientific, Singapore, 1993), p. 229 and references therein; W. de Boer, Prog. Part. Nucl. Phys. **33**, 201 (1994); W. de Boer, R. Ehret, and D. I. Kazakov, Z. Phys. C **67**, 647 (1995).
[13] S. Ambrosanio and B. Mele (in preparation).